https://doi.org/10.1093/plphys/kiad006 PLANT PHYSIOLOGY 2023: 191: 1751–1770

Plant Physiology®

Research Article

Roles of very long-chain fatty acids in compound leaf patterning in *Medicago truncatula*

Hongfeng Wang [1], Zhichao Lu [1], Yiteng Xu [1], Jing Zhang [1], Lu Han [1], Maofeng Chai [2], Zeng-Yu Wang [2], Xianpeng Yang [3], Shiyou Lu [4], Jianhua Tong [5], Langtao Xiao [5], Jiangqi Wen [6], Kirankumar S. Mysore [6] and Chuanen Zhou [1,*]

1 The Key Laboratory of Plant Development and Environmental Adaptation Biology, Ministry of Education, School of Life Sciences, Shandong University, Qingdao 266101, China
2 Grassland Agri-Husbandry Research Center, Qingdao Agricultural University, Qingdao 266109, China
3 College of Life Sciences, Shandong Normal University, Jinan 250014, China
4 State Key Laboratory of Biocatalysis and Enzyme Engineering, School of Life Sciences, Hubei University, Wuhan 430062, China
5 Hunan Provincial Key Laboratory of Phytohormones and Growth Development, Hunan Provincial Key Laboratory for Crop Germplasm Innovation and Utilization, Hunan Agricultural University, Changsha 410128, China
6 Institute of Agricultural Biosciences, Oklahoma State University, 3210 Sam Noble Parkway, Ardmore, Oklahoma 73401, USA

*Author for correspondence: czhou@sdu.edu.cn (C.Z.)
H.W. and C.Z. designed the research; H.W., Z.L., Y.X., and L.H. performed the experiments; J.Z. performed the RNA in situ hybridization experiments; M.C., Z.W., J.W., and K.S.M. contributed to the *Tnt1*-tagged mutants; X.Y., S.L., J.T., and L.X. analyzed the waxes and cutin composition and auxin level; H.W. and C.Z. wrote the paper. All the authors read and approved the contents of this manuscript.
The author responsible for distribution of materials integral to the findings presented in this article in accordance with the policy described in the Instructions for Authors (https://academic.oup.com/plphys/pages/General-Instructions) is Chuanen Zhou (czhou@sdu.edu.cn).

Abstract

Plant cuticles are composed of hydrophobic cuticular waxes and cutin. Very long-chain fatty acids (VLCFAs) are components of epidermal waxes and the plasma membrane and are involved in organ morphogenesis. By screening a barrelclover (*Medicago truncatula*) mutant population tagged by the transposable element of tobacco (*Nicotiana tabacum*) cell type1 (*Tnt1*), we identified two types of mutants with unopened flower phenotypes, named *unopened flower1* (*uof1*) and *uof2*. Both *UOF1* and *UOF2* encode enzymes that are involved in the biosynthesis of VLCFAs and cuticular wax. Comparative analysis of the mutants indicated that the mutation in *UOF1*, but not *UOF2*, leads to the increased number of leaflets in *M. truncatula*. *UOF1* was specifically expressed in the outermost cell layer (L1) of the shoot apical meristem (SAM) and leaf primordia. The *uof1* mutants displayed defects in VLCFA-mediated plasma membrane integrity, resulting in the disordered localization of the PIN-FORMED1 (PIN1) ortholog SMOOTH LEAF MARGIN1 (SLM1) in *M. truncatula*. Our work demonstrates that the *UOF1*-mediated biosynthesis of VLCFAs in L1 is critical for compound leaf patterning, which is associated with the polarization of the auxin efflux carrier in *M. truncatula*.

Introduction

The shoot apical meristem (SAM) is a structure at the tip of the shoot that is responsible for generating almost all of the above-ground tissue of the plant, such as leaves and flowers (Furner I and Pumfrey, 1992). According to the tunica-corpus theory, the SAM is divided into three distinct cell layers: the L1 epidermal, L2 subepidermal, and L3 layers (Schmidt, 1924; Sussex, 1989). The L1 epidermal is a composite tissue that forms the outer layers of plant organs, playing an important role in connecting the internal genetic factors and external environment signals (Barton, 2010; Perales and Reddy,

Received September 23, 2022. Accepted November 19, 2022. Advance access publication January 6, 2023

2012). During leaf development, cells of the L1 epidermal of the SAM divide anticlinally and then differentiate into pavement cells, guard cells, and trichomes.

A characteristic feature of the epidermis is that it is covered by the cuticle, a barrier to protect organisms away from stress (Lolle and Pruitt, 1999; Kunst and Samuels, 2009). In plants, the cuticle is composed of hydrophobic cuticular waxes and cutin (PostBeittenmiller, 1996; Samuels et al., 2008). Cuticular waxes are synthesized predominantly in epidermal cells and are mainly composed of very long-chain fatty acids (VLCFAs) and their derivatives, such as wax esters, alkanes, and aldehydes (Li-Beisson et al., 2013; Yeats and Rose, 2013). The C16- and C18-CoAs synthesized by plastids are elongated into VLCFAs in the endoplasmic reticulum (ER) membrane by a fatty acid elongase (FAE) complex, which is composed of β-ketoacyl-CoA synthase (KCS), β-ketoacyl-CoA reductase (KCR), β-hydroxy acyl-CoA dehydratase (HCD), and enoyl-CoA reductase (ECR) (Kunst and Samuels, 2009; Bernard and Joubes, 2013; Hegebarth and Jetter, 2017). The rate-limiting step of VLCFAs biosynthesis is a condensation of a malonyl-CoA unit to the acyl-CoA that is catalyzed by KCS (Lee and Suh, 2013; Yeats and Rose, 2013). In Arabidopsis (*Arabidopsis thaliana*), 21 *KCS* encoding genes are annotated and they have different or similar expression patterns and substrate specificities (Millar and Kunst, 1997; Trenkamp et al., 2004; Joubes et al., 2008). Among the *KCS*, mutation of the *FIDDLEHEAD* (*FDH*) leads to the fusion of leaves and floral organs (Lolle et al., 1992; Yephremov et al., 1999; Pruitt et al., 2000). In Antirrhinum (*Antirrhinum majus*), organ fusion phenotype can be induced by chloroacetamide, an inhibitor of β-ketoacyl-CoA synthases (Efremova et al., 2004). Furthermore, the VLCFAs are modified into primary alcohols by the alcohol-forming pathway and into ketones and secondary alcohols by the alkane-forming pathway, which are also important components of sphingolipids, seed triacylglycerols, and suberin (Li-Beisson et al., 2013). Cutin, the skeleton of the cuticle, is a plant-specific biopolymer that consists of C16 and/or C18 long-chain fatty acids and glycerol (Pollard et al., 2008; Dominguez et al., 2011). The formation of the extracellular cutin polymer is divided into three sequential steps. The first step is to synthesize cutin monomers in ER by the plastid-derived C16 and C18 fatty acids. Enzymes involved in this process are cytochrome P450 CYP77A6, long-chain acyl-CoA-synthetases (LACS), *sn*-2 glycerol phosphatase-acyltransferase (GPAT), ABERRANT INDUCTION OF TYPE THREE1 (ATT1), and HOTHEAD (HTH) (Shockey et al., 2002; Schnurr et al., 2004; Tang et al., 2007; Li-Beisson et al., 2009; Lu et al., 2009; Sauveplane et al., 2009; Pulsifer et al., 2012). Among them, *ATT1* encodes CYP86A2, a cytochrome P450 monooxygenase catalyzing fatty acid oxidation (Xiao et al., 2004). The *att1* mutant displays a loosely structured cuticle membrane, indicating CYP86A2 functions in cuticle development. Finally, the cutin monomers are exported from the ER to the nascent cuticular membrane through the lipid transfer proteins (LTP) and the ATP-binding cassette G (ABCG) transporters (Bird et al., 2007; Debono et al., 2009; Bessire et al., 2011; Kim et al., 2012), and polymerization is catalyzed by the α/β-hydrolase BODYGUARD (BDG) and acyltransferase DEFECTIVE IN CUTICULAR RIDGES (DCR) (Kurdyukov et al., 2006; Panikashvili et al., 2009).

Auxin regulates many developmental processes in plants. During leaf development, auxin coordinates the phyllotaxis of leaf initiation from the SAM and determines the location of serrations and the initiation of leaflets from the margin of leaf primordia (Barkoulas et al., 2008; Koenig et al., 2009; Shwartz et al., 2016). Auxin transport at the shoot apical is mediated by the PIN-FORMED (PIN) family members (Shi et al., 2017). PIN1 is one of the auxin transporters with a polar localization within the SAM responsible for forming auxin gradients in the L1 that in turn control the initiation of leaf primordia and the formation of leaf serrations (Benková et al., 2003; Xiong and Jiao, 2019). The PIN1 polar targeting and cell polarity proliferation/expansion depend largely on the composition of the plasma membrane, such as VLCFAs and their derivatives. *PASTICCINO1* (*PAS1*) encodes a large molecular weight member of the immunophilin-type binding protein family that is required for VLCFA synthesis (Vittorioso et al., 1998). Loss of *PAS1* function results in the reduction of sphingolipids levels and the mistargeting of the PIN1, resulting in the local alteration of polar auxin distribution in the embryo apex cells (Roudier et al., 2010). *STEROL METHYLTRANSFERASE1* (*SMT1*) encodes an enzyme that is required for appropriate sterol levels (Diener et al., 2000). *SMT1* is involved in the C24 alkylation of sterols, and the columella cells of the *smt1* mutant display defective apical-basal polarity and disturbed localization of the PIN proteins (Schrick et al., 2002; Willemsen, 2003). Furthermore, the rice (*Oryza sativa*) *ONION1* (*ONI1*), an ortholog of *FDH*, is also required for VLCFAs synthesis and correct fatty acid composition, and loss of *ONI1* function mutants show the abnormal L1, causing altered auxin distribution in the shoot (Ito et al., 2011; Takasugi and Ito, 2011).

Although much progress on cuticle formation and its functions on plant development has been made in different species, however, the roles of cuticle components, especially VLCFAs and their derivatives, in compound leaf patterning are still unclear. In this study, we identified two types of mutants with unopened flower phenotype in barrelclover (*Medicago truncatula*), named *unopened flower1* (*uof1*) and *uof2*. Both *UOF1* and *UOF2* encoded enzymes that were involved in the biosynthesis of VLCFAs and the formation of the cuticle. Both *uof1* and *uof2* had a reduced amount of VLCFAs and cuticular wax, however, only the leaves of *uof1* mutants showed an increased number of leaflets. Comparison of the expression pattern between *UOF1* and *UOF2* indicated that *UOF1*, instead of *UOF2*, was specifically expressed in epidermal cells of different organs. We presented a model for the roles of *UOF1*-mediated biosynthesis of VLCFAs in L1 in regulation of elaboration of compound leaves, which is associated with proper polar localization of PIN1 ortholog in *M. truncatula*.

Results

Identification of two types of unopened flower mutants in *M. truncatula*

To identify regulators that control compound leaf morphogenesis and flower development in legumes, about 22,000 independent lines of the *Tnt1*-tagged *M. truncatula* mutant population (Tadege et al., 2008) were screened. Two types of mutants with similar unopened flower phenotypes were identified. These mutants were named *unopened flower1* (*uof1*) and *uof2*, respectively. The flower in wild-type had normally expanded petals at the early development stage (Figure 1, A and B; Supplemental Figure 1A), however, the corolla of *uof1-1* flowers was tightly enclosed by the enlarged sepals, preventing petal expansion, and the stigma expands outward (Figure 1, E and F; Supplemental Figure 1B). In addition, the petals of *uof2-1* were also manacled by sepals resulting in the closed flower and the exposed stigma (Figure 1, I and J; Supplemental Figure 1C). At the late development stage, wild-type plants could develop seed pods (Figure 1, C and D). In both *uof1-1* and *uof2-1* mutants, one or two pod spirals were observed, but they normally dropped later due to lack of pollination, leading to the sterility in mutant plants (Figure 1, G, H, K, and L).

To further investigate the reason for sterility in *uof1* and *uof2* flowers, the developmental processes of floral organ primordia between the wild-type and mutants were compared by a scanning electron microscope (SEM). At stage 6, the sepal, petal, and stamen primordia were completely formed and the central carpel became visible in the wild-type, *uof1-1*, and *uof2-1* flowers, indicating that the initiation of the primordia of the floral organs is normal in both wild-type and mutants (Supplemental Figure 1, D–F). Moreover, pollen staining revealed that pollens in mutants were fertile, similar to those of the wild-type (Supplemental Figure 1, G–I). These observations suggest that unopened flowers induced by the restraint of sepals in *uof1* and *uof2* lead to the increased physical distance between stigma and anthers, resulting in the sterility.

Molecular cloning and genetic complementation analysis

To identify the genes responsible for the unopened flower phenotype of *uof1* and *uof2* mutants, we first analyzed the flanking sequences derived from the *uof1* mutants as described (Tadege et al., 2008), and found that one sequence was associated with the unopened flower phenotype of *uof1* mutants. Then, we used this sequence to align in the *M. truncatula* genome database. A gene with a full-length genomic sequence of 3349 nucleotides was obtained (Figure 2A). Further analysis showed that the *Tnt1* insertions were located at the second exon in *uof1-1*, *uof1-2*, and *uof1-3*, and at the third exon in *uof1-4* (Figure 2A). Subsequent co-segregation analyses on the progeny of self-pollinated heterozygous *uof1-1*/+ and *uof1-2*/+ plants were performed, respectively (Supplemental Figure 2, A–D). The ratio between wild-type-like plants and *uof1* mutants was approximately 3:1 (Supplemental Figure 2, A and B), suggesting that the *uof1* mutant phenotype was caused by the mutation of a single recessive gene. Furthermore, genomic PCR and reverse transcription PCR (RT-PCR) analysis showed that homozygous insertion of *Tnt1* resulted in the interruption of *UOF1* expression (Figure 2, B and C). Phylogenetic analysis revealed that UOF1, the ortholog of *Arabidopsis* KCS10/FDH and a rate-limiting enzyme of VLCFAs synthesis, was required for the correct formation of the cuticle (Supplemental Figures 3 and 4). For genetic complementation, a vector containing the *UOF1* genomic sequence and its native promoter was introduced into *uof1-1* mutants using *Agrobacterium tumefaciens*-mediated transformation. Phenotypic analysis indicated that complementary *UOF1* expression fully rescued the unopened flower phenotype of *uof1-1* mutants (Figure 2, G and H). These data indicate that the loss-of-function mutation of *UOF1* is responsible for the unopened flower phenotype of the *uof1* mutants.

The *UOF2* gene was also cloned by PCR-based genotyping of flanking sequence tags in the segregating populations. Alignment of the coding sequence and full-length genomic sequence of the *UOF2* gene indicated that *UOF2* was composed of only one exon, and the *Tnt1* retrotransposons were inserted at positions 243 and 1151 bp of *uof2-1* and *uof2-2*, respectively (Figure 2D). Co-segregation analyses showed that the *uof2* mutant phenotype was also caused by a single recessive nuclear gene mutation (Supplemental Figure 2, E–H). Genomic PCR and RT-PCR results revealed that all *uof2* mutant lines were knockout alleles of the *UOF2* gene due to *Tnt1* insertions (Figure 2, E and F). Phylogenetic analysis showed that *UOF2* encodes a member of the CYP86A subfamily of cytochrome P450-dependent fatty acid ω-hydroxylase, and it is homologous to *Arabidopsis* CYP86A2/ATT1, implying its function in cuticle formation (Supplemental Figures 5 and 6). Further genetic complementation confirmed that complementary *UOF2* expression fully rescued the unopened flower phenotype of *uof2-1* mutants (Figure 2I).

The defects in wax load and cuticle permeability in the *uof* mutants

To investigate whether *UOF1* and *UOF2* play roles in the development of cuticles, we examined the epidermal phenotype of *uof1-1* and *uof2-1* mutants. Firstly, the toluidine blue (TB) staining test was executed to assay the cuticle permeability. The results showed that the flowers and leaves of *uof1-1* and *uof2-1* mutants displayed increased staining compared with that in wild-type plants (Figure 3, A–F), indicating that cuticle permeability was increased in *uof1-1* and *uof2-1* mutants. Secondly, the leaf surface was examined by SEM to check the possible changes in wax. Compared with the wild-type leaves, the epidermal wax crystals load of *uof1-1* and *uof2-1* mutants was substantially reduced (Figure 3, G–I). In agreement with this notion, the leaves of *uof1-1* and *uof2-1* mutants showed a more rapid water loss than

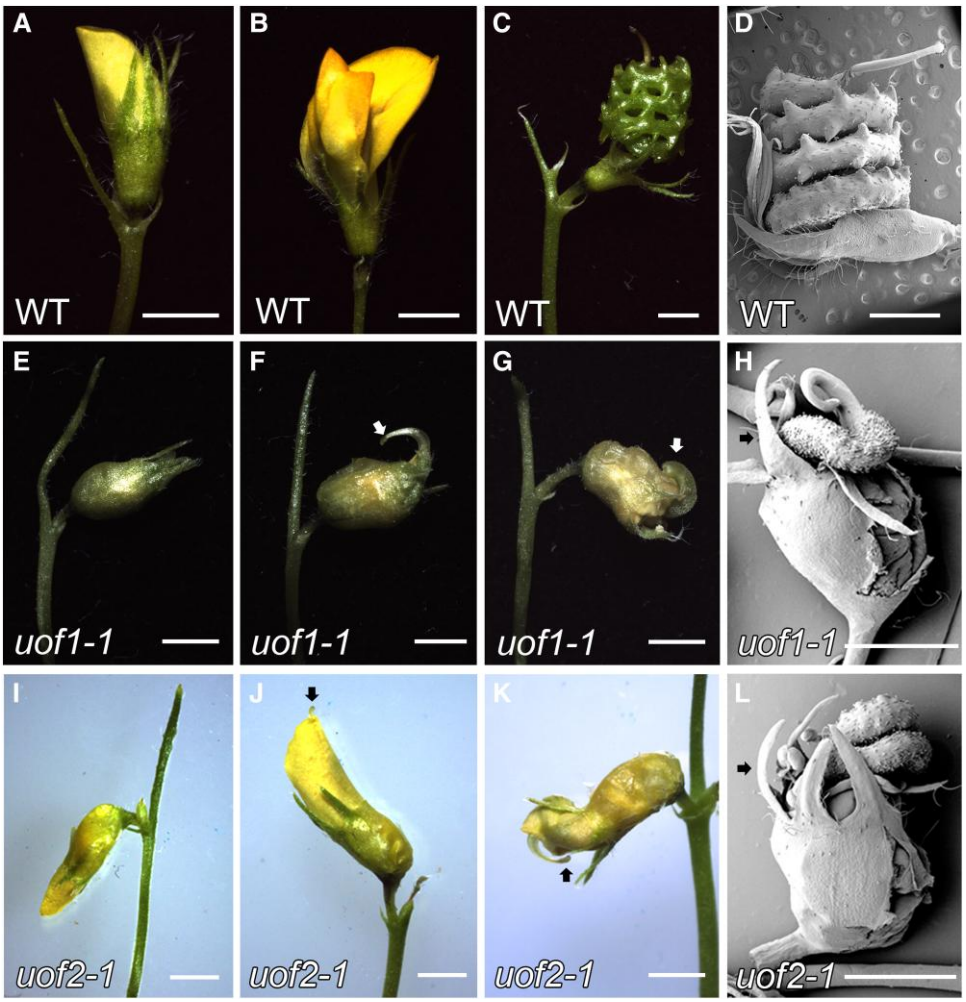

Figure 1 Phenotypic analysis of the *uof1-1* and *uof2-1* flowers. A–C, Flowers of wild-type plants at different developmental stages. Early stage flower (A), mature flower (B), and pod (C) of wild-type plants are shown. D, SEM analysis of the pod of wild-type plant. E–G, Flowers of *uof1-1* mutants. Early stage flower (E), mature flower (F), and late stage flower (G) of *uof1-1* mutants are shown. Arrows in (F and G) indicate the outward expanded stigmas in *uof1-1* mutants. H, SEM analysis of the late stage flower of *uof1-1* mutants. The arrow in (H) indicates the enclosed sepals of the *uof1-1* flower. I–K, Flowers of *uof2-1* mutants. Early stage flower (I), mature flower (J), and late stage flower (K) of *uof2-1* mutants are shown. Arrows in (J and K) indicate the outward expanded stigmas in *uof2-1* mutants. L, SEM analysis of the late stage flower of *uof2-1* mutants. The arrow in (L) indicates the enclosed sepals of the *uof2-1* flower. Bars, 2 mm in (A–L).

those of the wild-type (Figure 3J). To further characterize the defects in epidermal wax, the total wax load and wax constituents were analyzed. Compared with the wild-type, the total amount of wax on leaves was significantly decreased by 23% in *uof1-1* and 55% in *uof2-1* (Figure 3K). Most of the changes in the amount of leaf wax in *uof1-1* and *uof2-1* were caused by the reduction of C30 and C28 alcohols, and C30 aldehydes (Figure 3M), which were the dominant wax components throughout leaf development. However, the loss-of-function of *UOF1* and *UOF2* resulted in a slight increase in the cutin amount (Figure 3, L and N). These observations demonstrate that the defects in cuticle in *uof1* and *uof2* mutants are mainly caused by the loss of very long-chain alcohols and aldehydes.

In addition, it was reported that many mutants lacking epidermal wax exhibit organ adhesion or fusion in the shoot (Yephremov et al., 1999; Wellesen et al., 2001; Ito et al., 2011; Panikashvili et al., 2011). Morphological analysis showed that organ adhesions occur between flowers and leaves and between leaflets in both *uof1* and *uof2* mutants when the leaves and flowers just developed in the apical shoot tips (Supplemental Figure 7). However, the adhesion between organs was recovered along with the plant growth. These results indicate that *UOF1* and *UOF2* play conserved roles in regulating leaf and floral organ separation.

UOF1, but not *UOF2*, is required for compound leaf patterning and leaf margin formation

In the wild-type, all adult leaves were in trifoliate form with a terminal leaflet and two lateral leaflets (Figure 4A). All four alleles of

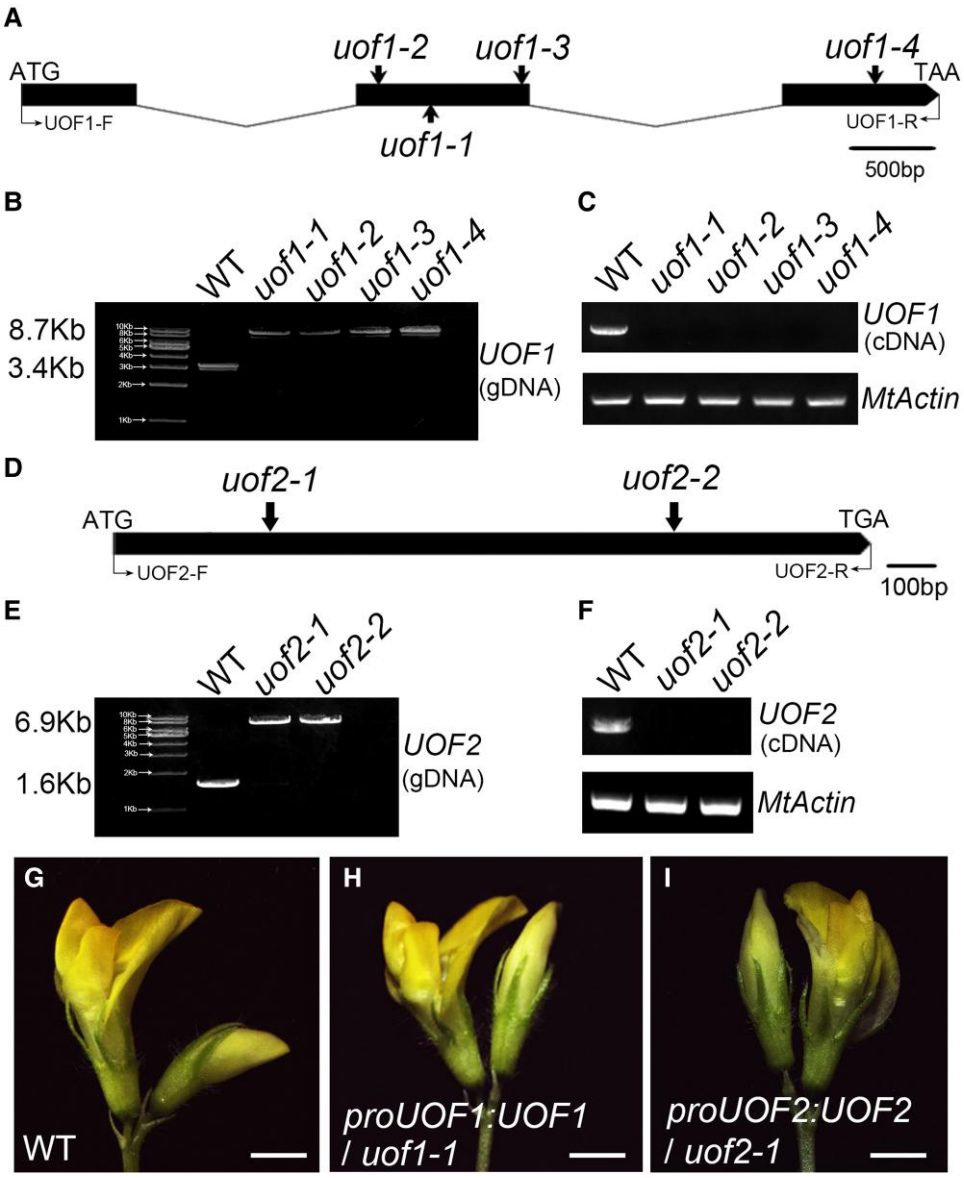

Figure 2 Molecular cloning of the *UOF1* and *UOF2* genes and genetic complementation analysis. A, The gene structure of *UOF1* and *Tnt1* insertion sites of different *uof1* alleles. Black boxes represent exons and lines represent introns. The start codon (ATG) and stop codon (TAA) are indicated. B, PCR amplification of the *UOF1* genomic sequences from wild-type and different *uof1* alleles using primers UOF1-F/UOF1-R. A single *Tnt1* insertion (~5.3 kb) was detected in each *uof1* mutant line. C, RT-PCR analysis of *UOF1* transcripts in the wild-type and different *uof1* alleles using primers UOF1-F/UOF1-R. *MtActin* was used as the control. D, The gene structure of *UOF2* and *Tnt1* insertion sites of different *uof2* alleles. The start codon (ATG) and stop codon (TGA) are indicated. E, PCR amplification of the *UOF2* genomic sequences from wild-type and different *uof2* alleles using primers UOF2-F/UOF2-R. A single *Tnt1* insertion (~5.3 kb) was detected in each *uof2* mutant line. F, RT-PCR analysis of *UOF2* transcripts in wild-type and different *uof2* alleles using primers UOF2-F/UOF2-R. G, Flower of the wild-type plants. H and I, Flowers of *uof1-1* and *uof2-1* mutants complemented with *proUOF1:UOF1* (H) and *proUOF2:UOF2* (I), respectively. Bars, 2 mm in (G–I).

UOF1 showed a substantial increase in leaflets number that about 50% of the adult leaves produced one to three ectopic leaflets (Figure 4, B–E and G; Supplemental Figure 8, A–C and E). Phenotypic observation confirmed that complementary *UOF1* expression fully rescued the defects in leaf patterning and leaf margin of *uof1-1* mutant (Supplemental Figure 8, D and E). However, the compound leaf patterning in *uof2-1* mutants was unchanged (Figure 4, F and G). Moreover, the leaves of the wild-type and *uof2-1* mutants formed a serrated leaf margin (Figure 4, H–J and N–P), but the leaf margin of *uof1* mutants was relatively smooth (Figure 4, K–M; Supplemental Figure 8, F–H). These observations suggest that loss-of-function in *UOF1* affects the development of both compound leaf and leaf margin serrations. To investigate the genetic relationship between *UOF1* and *UOF2*, we generated the *uof1-1 uof2-1* double mutant by crossing. The leaf type proportion of *uof1-1 uof2-1* was similar to

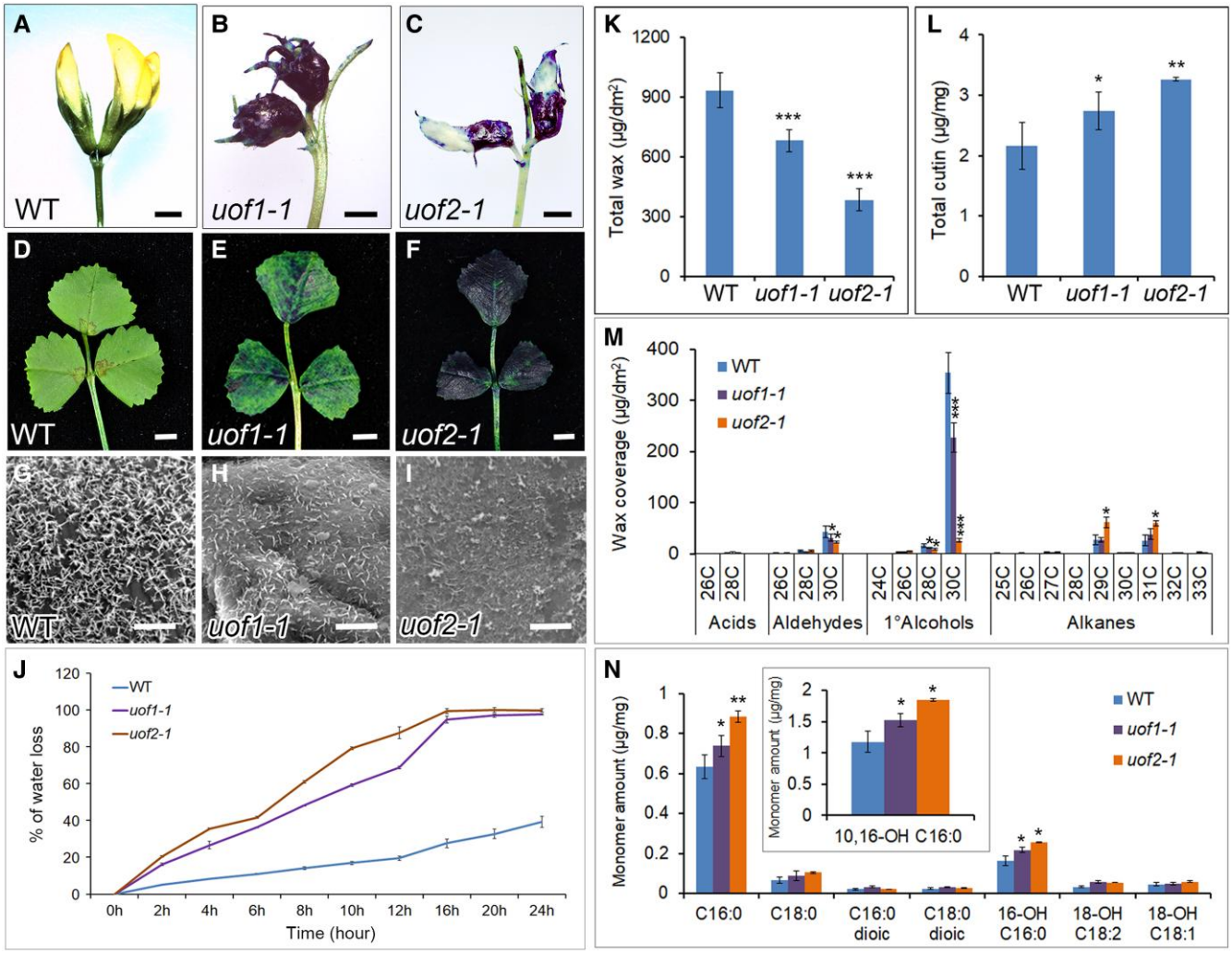

Figure 3 Mutation of *UOF1* and *UOF2* leads to defects in cuticle development. A–F, Toluidine blue stained flowers (A–C) and leaves (D–F) of wild-type, *uof1-1*, and *uof2-1* plants. Bars, 2 mm in (A–C) and 5 mm in (D–F). G–I, SEM analyses of the cuticular wax crystals in leaves of wild-type (G), *uof1-1* (H), and *uof2-1* (I) plants. Bars, 10 μm in (G–I). J, Water loss rates of wild-type, *uof1-1*, and *uof2-1* leaves were measured. Values are the mean and SD of three replicate assays. K and L, The contents of total wax (K) and cutin (L) in the leaves of wild-type, *uof1-1*, and *uof2-1* plants. Values are the means and SD of three biological replicates. M and N, Cuticular wax (M) and fatty acid (N) composition in leaves of wild-type, *uof1-1*, and *uof2-1* plants. Values are the means and SD of three biological replicates. $^{*}P < 0.05$; $^{**}P < 0.01$; $^{***}P < 0.001$. The two-sided Student's *t* test was used to estimate if the difference is significant.

that of *uof1-1* mutant (Supplemental Figure 8E). In some cases, the compound leaf patterning of *uof1-1 uof2-1* was the same as that of the *uof1-1* mutant (Supplemental Figure 8, J–L). Moreover, the leaf margin and flowers in *uof1-1 uof2-1* double mutants resembled those of *uof1-1* (Supplemental Figure 8, I and M–O). These observations indicate that *uof1* was genetically epistatic to *uof2* in both leaf and flower development.

Expression patterns of *UOF1* and *UOF2*

To explore the possible reason for the distinct compound leaf patterning between *uof1* and *uof2* mutants, the expression patterns of *UOF1* and *UOF2* were compared. Reverse transcription quantitative PCR (RT-qPCR) data showed that *UOF1* was expressed at higher levels than *UOF2* in most organs (Figure 5A; Supplemental Figure 9A). To analyze the expression levels in more detail, the *proUOF1:GUS* and *proUOF2:GUS* transgenic plants were obtained. Consistent with the RT-qPCR results, *UOF1* and *UOF2* showed a similar expression pattern, in which GUS signals were detected in sepals of flowers and whole leaves (Figure 5, B–E). To gain better spatial expression patterns of *UOF1* and *UOF2*, RNA in situ hybridization was performed on the shoot apex of wild-type plants. The data showed that *UOF1* transcripts were specifically expressed in the L1 of SAM, emerging leaf primordia, and floral meristem (Figure 5, F and G). However, *UOF2* transcripts were detected in the center of SAM and floral meristem with relatively low expression levels (Figure 5, H and I). As negative controls, the sense probes did not give any

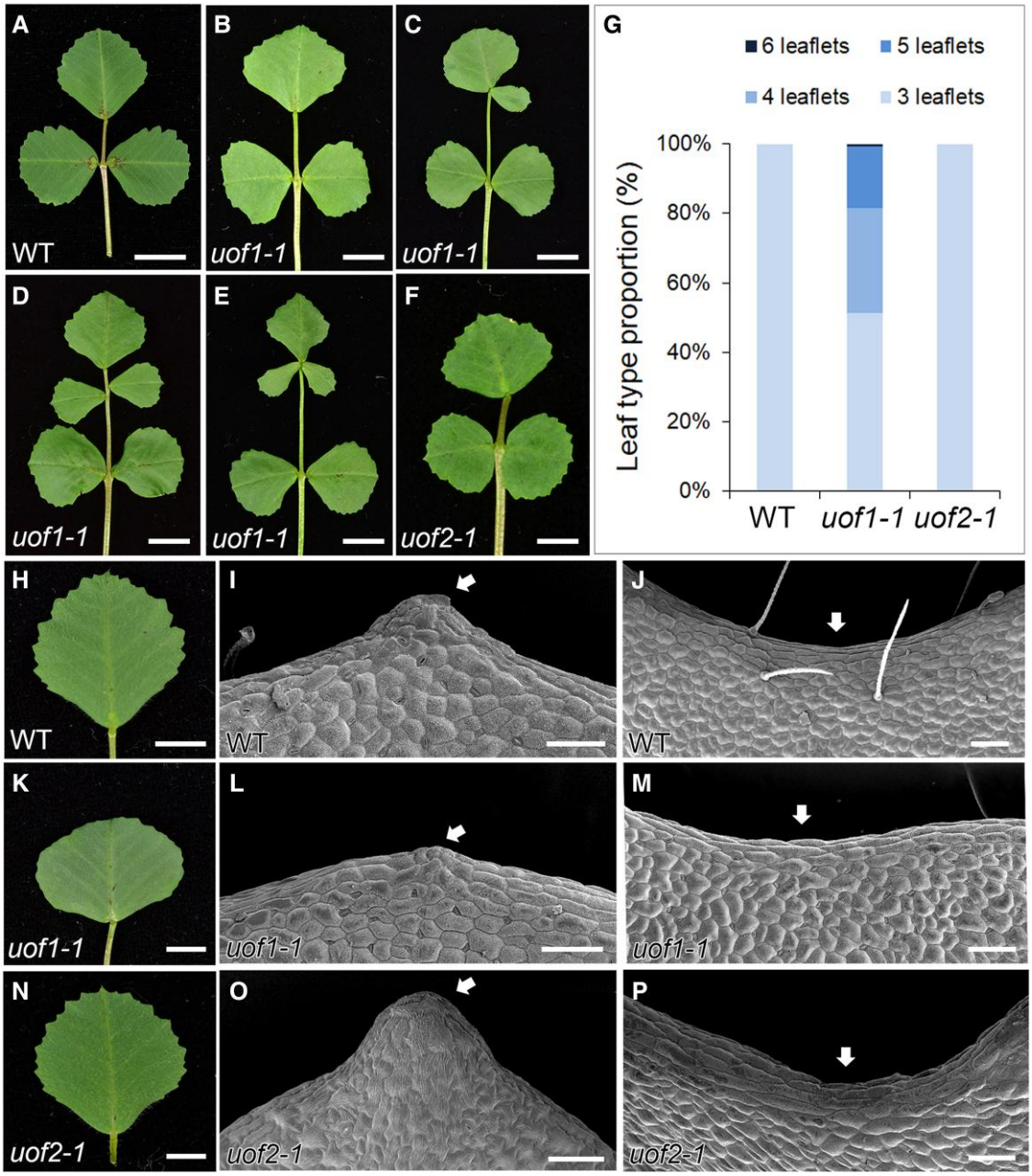

Figure 4 The *uof1-1* mutants show defects in compound leaf development. Adult leaves of wild-type (A), *uof1-1* (B–E), and *uof2-1* (F) plants. Leaflet number is substantially increased in some leaves of *uof1-1* mutant (C–E). Bars, 1 cm in (A–F). G, Leaf type proportion in wild-type ($n = 150$), *uof1-1* ($n = 132$), and *uof2-1* ($n = 125$) plants. Development of leaf margins in wild-type (H–J), *uof1-1* (K–M), and *uof2-1* (N–P). Observations of marginal cells at the teeth tips (I, L, and O) and leaf sinus (J, M, and P) in wild-type (I and J), *uof1-1* (L and M), and *uof2-1* (O and P) by SEM. Arrows indicate the relatively smooth leaf margin serrations and sinus in the *uof1-1* mutant (L and M) compared with the wild-type (I and J) and *uof2-1* mutant (O and P). Bars, 5 mm in (H, K, and N) and 100 μm in (I–J, L–M, and O–P).

hybridization signals (Figure 5, J and K). To further confirm the L1-specific expression pattern of *UOF1*, wild-type plants transformed with the *proUOF1:GFP* reporter were obtained. GFP signals were detected not only in the L1 of SAM and leaf primordia but also in developing leaves and leaf margin serrations (Figure 5, L–P). Strong GFP signals were also detected in the epidermis of floral primordia, anthers, and seeds (Supplemental Figure 9, B–G). These observations demonstrate that *UOF1* and *UOF2* display the distinct expression patterns, implying that the specific transcription of *UOF1* in the L1 may be the key to the formation of compound leaf patterning.

The expression pattern of *SMOOTH LEAF MARGIN1* (*SLM1*) is unchanged in *uof1*

Our previous study showed that *SLM1*, the *PIN1* ortholog in *M. truncatula*, was apically localized in the L1 of the

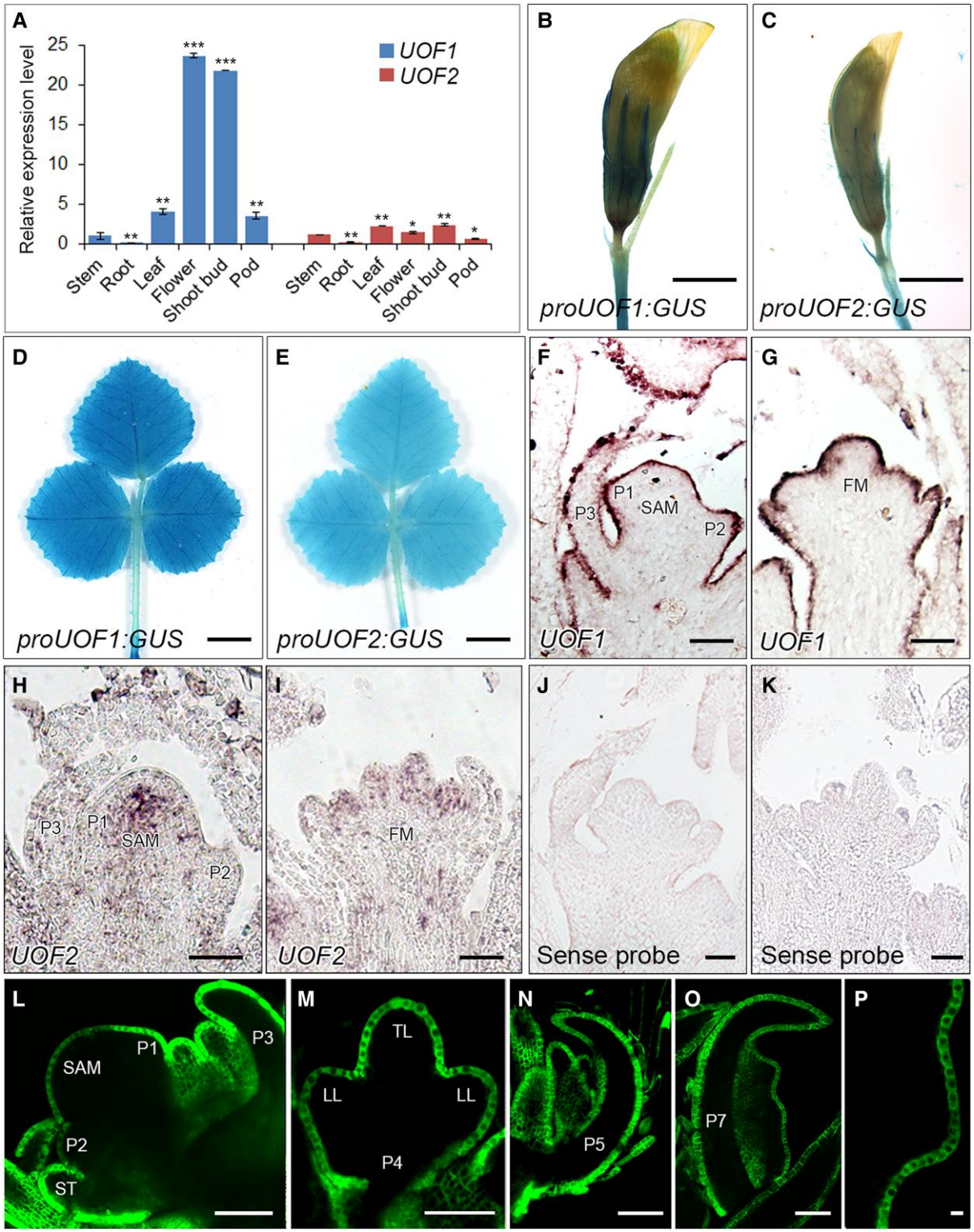

Figure 5 The expression patterns of *UOF1* and *UOF2* genes. A, The relative expression levels of *UOF1* and *UOF2* genes in different wild-type tissues. Values are the means and SD of three biological replicates; $^{*}P < 0.05$; $^{**}P < 0.01$; $^{***}P < 0.001$. The two-sided Student's *t* test was used to estimate if the difference is significant. B–E, Promoter-GUS fusion studies of *UOF1* and *UOF2* expression in transgenic plants. *UOF1* and *UOF2* promoters driven GUS were expressed in the flowers (B and C) and adult leaves (D and E). Bars, 2 mm in (B and C) and 5 mm in (D and E). F–I, The expression patterns of *UOF1* (F and G) and *UOF2* (H and I) were detected by RNA in situ hybridization. SAM, shoot apical meristem; P, leaf primordium; FM, floral meristem. J, K, The sense probes were hybridized and used as control. Bars, 50 μm in (F–K). L–P, Promoter-GFP fusion study of the *UOF1* expression pattern in transgenic plants. GFP signals were specifically localized to the plasma membrane of epidermal cells of SAM and leaf primordia (L–O) and leaf margin serration cells (P). ST, stipule primordium; TL, terminal leaflet primordium; LL, lateral leaflet primordia. Bars, 50 μm in (L–P).

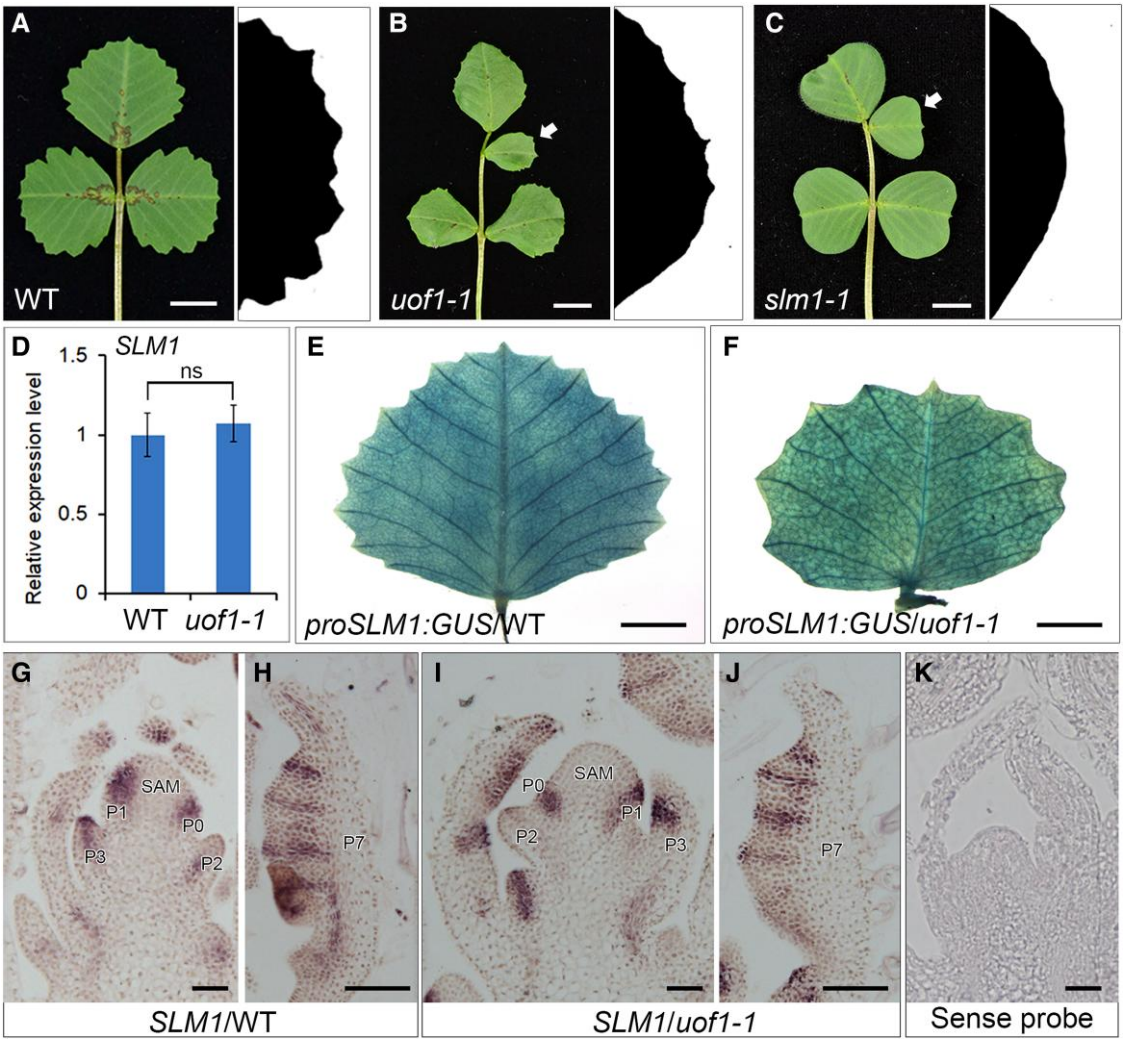

Figure 6 Developmental defects in *uof1* resemble those in *slm1*. A–C, Leaf and leaf margin phenotypes of wild-type (A), *uof1-1* (B), and *slm1-1* (C) plants. Compared with the wild-type leaf (A), the *uof1-1* and *slm1-1* mutant exhibit similar defects in compound leaf patterning (B and C; left) and leaf margin development (B and C; right). White arrows in (B and C) indicate the ectopic leaflets in *uof1-1* and *slm1-1* mutants. D, The relative expression levels of *SLM1* in wild-type and *uof1-1* leaves were detected by RT-qPCR. There was no significant difference in *SLM1* expression between wild-type and *uof1-1* mutants. Values are the means and SD of three biological replicates. E and F, The expression patterns of *SLM1* in fully expanded leaves of the wild-type (E) and *uof1-1* mutants (F), as determined by detecting the *proSLM1:GUS* activity. G–J, The expression patterns of *SLM1* in shoot buds (G and I) and leaf primordia (H and J) of the wild-type and *uof1-1* mutants, as determined by RNA in situ hybridization. SAM, shoot apical meristem; P, leaf primordium. K, The sense probe of *SLM1* was hybridized and used as control. Bars, 1 cm in (A–C), 5 mm in (E and F), and 50 μm in (G–K).

SAM and leaf primordia (Zhou et al., 2011). In addition, loss-of-function of *SLM1* led to increased leaflet number and smoothed leaf margin, which was also observed in *uof1* mutant (Figure 6, A–C). To investigate the possible relationship between *UOF1* and *SLM1* gene, RT-qPCR was performed to analyze the expression of *SLM1*. Compared with the wild-type, the expression level of *SLM1* was unchanged in *uof1-1* mutants (Figure 6D). To further investigate whether the leaf developmental defects in *uof1-1* were caused by the disruption of *SLM1* expression pattern, the *proSLM1:GUS* construction was introduced into wild-type and *uof1-1* plants, respectively. However, GUS staining showed the similar expression patterns of *SLM1* between wild-type and *uof1-1* mutants (Figure 6, E and F). Then, RNA in situ hybridization was performed in the shoot apex of wild-type and *uof1-1* mutants. In the wild-type, *SLM1* mRNA was detected in SAM at the sites where leaf primordia gave rise and in the developing leaf primordia (Figure 6, G and H). The *uof1-1* mutant showed the same *SLM1* expression pattern as those in the wild-type (Figure 6, I and J). As a negative control, the sense *SLM1* probe did not give any hybridization signal (Figure 6K). These results indicate that the mutation of *UOF1* does not change the expression level and pattern of *SLM1*.

Global changes in gene expression in *uof1-1* mutant

To further explore the roles of *UOF1* in the formation of compound leaf patterning, RNA-sequencing analyses were performed. Comparing the whole transcriptome profiles

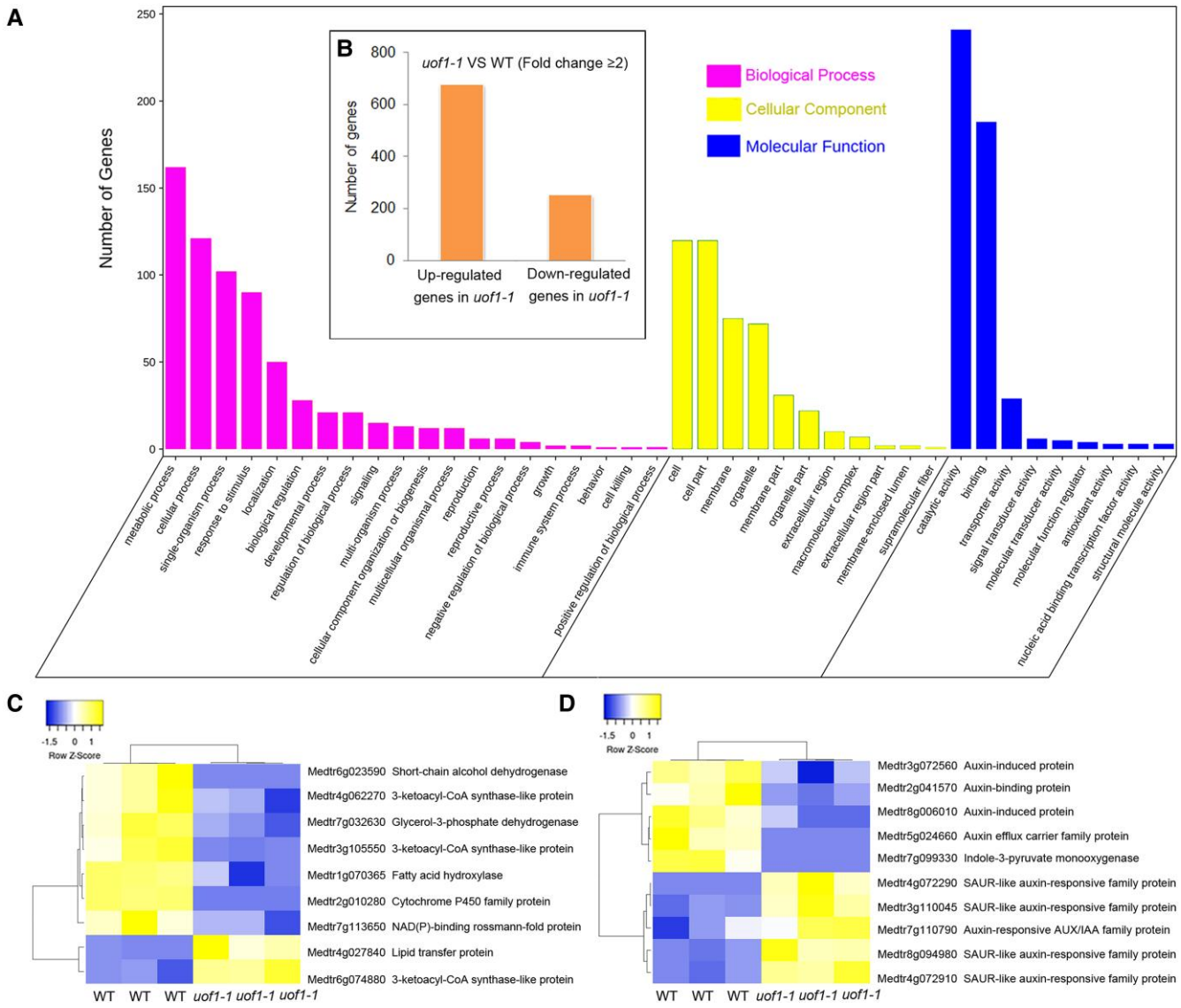

Figure 7 Comparison of wild-type and *uof1-1* transcriptomes. A, GO enrichment of genes with changed expression in shoot buds of *uof1-1* mutants. B, The number of differentially expressed genes (DEGs, ≥2-fold change) of *uof1-1* compared with wild-type. C, Heatmap of fatty acids biosynthesis related DEGs. D, Heatmap of auxin biosynthesis, signaling, and response-related DEGs.

between wild-type and *uof1-1* mutants, a total of 930 differentially expressed genes (DEGs) (ratio ≥ 2) were identified, among which 679 genes were up-regulated and 251 were down-regulated in the leaves of *uof1-1* mutants relative to the wild-type (Figure 7B; Supplemental Table 2). Gene ontology (GO) analysis revealed that the changed genes were highly enriched for biological processes associated with metabolic processes, cellular processes, single-organism processes, response to stimulus, and localization, and were also enriched for cellular component and molecular function categories related to cell part, membrane part, and catalytic activity (Figure 7A; Supplemental Figure 10).

Many down-regulated genes in the *uof1-1* mutants encode enzymes that were involved in the biosynthesis of VLCFAs and their derivatives, and membrane components (Figure 7C). In addition to VLCFAs, auxin biosynthesis and auxin-induced genes were also substantially down-regulated in the *uof1-1* mutants (Figure 7D). These results suggest that VLCFA-mediated plasma membrane integrity and auxin content may decrease in *uof1* mutants.

PIN1 localization is changed in *uof1* mutant

As *UOF1* was specifically expressed in the L1 cells and involved in the synthesis of VLCFAs which were also major components of the plasma membrane, we hypothesized that the plasma membrane in L1 was defective. The Arabidopsis PLASMA MEMBRANE INTRINSIC PROTEIN2A (AtPIP2A) is a member of the plasma membrane intrinsic protein subfamily and specifically localizes to the plasma membrane (Verdoucq et al., 2008; Wudick et al., 2015; Yoo et al., 2016; Byrt et al., 2017). To verify this, the marker *35S:AtPIP2A-GFP* (Luo and Nakata, 2012) was introduced into

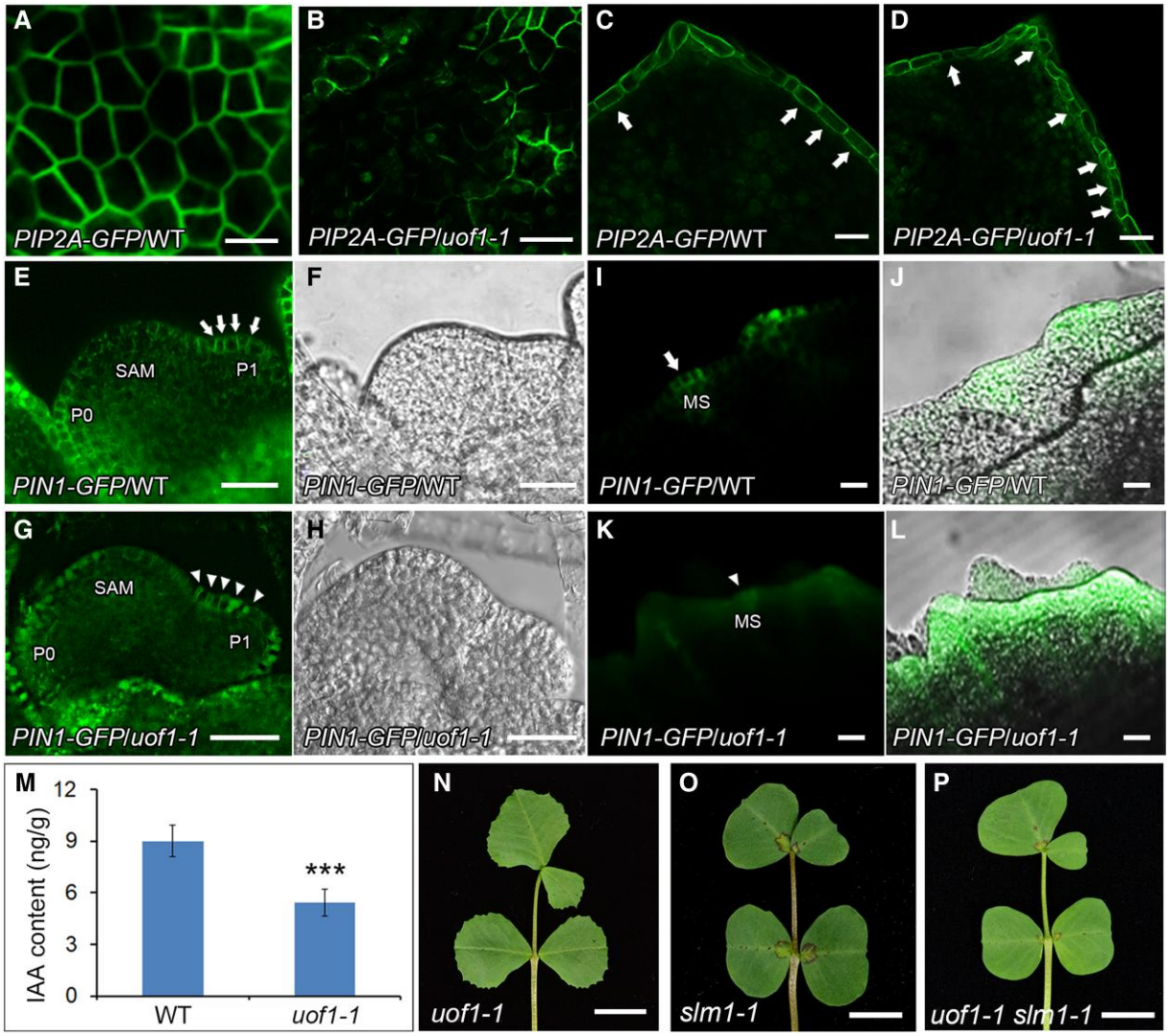

Figure 8 The localization of PIN1/SLM1 in wild-type and *uof1* mutants. A–D, The integrity of the plasma membrane of leaf epidermal cells (A and B) and leaf marginal cells (C and D) of wild-type and *uof1-1* mutants were analyzed, as determined by detecting the *35S:AtPIP2A-GFP* marker. Arrows in (C) mark the continuous GFP signal in leaf marginal cells of wild-type, and in (D) mark the intermittent GFP signal in leaf marginal cells of *uof1-1* mutants. Bars, 50 μm in (A–D). E–L, Distribution of the *proAtPIN1:AtPIN1-GFP* marker (green signal) in leaf primordia (E and G) and leaf margin serrations (I and K) of wild-type and *uof1-1* mutants. Arrows mark the polar localization of PIN1 in leaf primordia (E) and leaf margin serration (I) of wild-type, while arrowheads mark the disturbed polar localization of PIN1 in leaf primordia (G) and leaf margin serration (K) of the *uof1-1* mutants. The bright fields of SAM and leaf primordial of (E and G) are shown in (F and H), the merged images between GFP signals and bright fields of leaf margin serrations are shown in (J and L). SAM, shoot apical meristem; P, leaf primordium; MS, leaf margin serration. Bars, 50 μm in (E–H) and 100 μm in (I–L). M, The concentration of free indole-3-acetic acid (IAA) in 4-week-old leaves of wild-type and *uof1-1* mutants. Values are the means and SD of three biological replicates; $^{***}P < 0.001$. The two-sided Student's *t* test was used to estimate if the difference is significant. N–P, Leaves of *uof1-1* (N), *slm1-1* (O), and *uof1-1 slm1-1* double mutant (P). Bars, 1 cm in (N–P).

wild-type and *uof1-1* mutants. In wild-type, the leaf epidermal cells and margin cells showed continuous GFP signals in the plasma membrane (Figure 8, A and C). However, an intermittent GFP signal was presented in the *uof1-1* mutants (Figure 8, B and D), indicating that the integrity of the plasma membrane of L1 is largely defective in the *uof1-1* mutants. Furthermore, SEM analysis showed that the epidermal cells of leaves were indistinguishable between *uof1-1* and wild-type (Supplemental Figure 11), suggesting that the intermittent GFP signal in the *uof1-1* was not caused by leaf morphological changes. These observations indicate that loss of *UOF1* function leads to defects in plasma membrane integrity in L1 cells.

It was reported that polar localized PIN1-mediated auxin maxima in L1 are critical for the proper initiation of leaf primordia and the formation of leaf serrations (Reinhardt et al., 2003; Heisler et al., 2005; de Reuille et al., 2006). Our previous study showed that SLM1 is functionally equal to AtPIN1 (Zhou et al., 2011). Therefore, the *proAtPIN1:AtPIN1-GFP*

reporter was introduced into wild-type and *uof1-1* mutants to investigate whether the defective plasma membrane affected the polar localization of *PIN1*. In wild-type, PIN1 was apically localized at the L1 of the SAM and leaf primordia (Figure 8, E and F). However, the polar localization of PIN1 was disturbed in *uof1-1* (Figure 8, G and H). Such defective localization of PIN1 was also observed in the marginal cells at the tip of serrations in *uof1-1* leaves (Figure 8, I–L). These results demonstrate that the mutation of *UOF1* leads to the defective in plasma membrane, resulting in the disordered polar localization of PIN1. To further investigate the role of auxin in *uof1* mutant, the endogenous auxin level was determined. The free indole-3-acetic acid (IAA) concentration of the *uof1-1* mutants was significantly lower than that of the wild-type plants (Figure 8M). In addition, genetic interaction analysis showed that the leaf patterning of *uof1-1 slm1-1* double mutants was similar to those of *slm1* (Figure 8, N–P), suggesting that *slm1* is epistatic to *uof1* in terms of leaf complexity. However, the *uof1-1 slm1-1* double mutants still exhibited the organ adhesion and the defects in cuticular wax (Supplemental Figure 12), indicating that disruption of *SLM1* does not change the abnormal wax biosynthesis in *uof1-1*.

SINGLE LEAFLET1 (*SGL1*) and class I *MtKNOX* (*MtKNOXI*) in L1 play limited roles in the regulation of the indeterminacy during leaf formation

Previous studies showed that the *FLORICAULA* (*FLO*)/*LEAFY* (*LFY*) putative ortholog *SGL1* functioned in place of *KNOXI* to regulate compound leaf development in *M. truncatula* (Champagne et al., 2007; Wang et al., 2008). *SGL1* was expressed in the SAM and emerging leaf primordia, and the leaves of *sgl1* mutants were simple rather than compound (Figure 9, A and B; Wang et al., 2008). To investigate the genetic relationship between *UOF1* and *SGL1*, the *uof1-1* was crossed with the *sgl1-1* mutant. Similar to *sgl1-1*, the *uof1-1 sgl1-1* double mutant formed simple leaves (Figure 9C), indicating that *sgl1* was genetically epistatic to *uof1* in the regulation of compound leaf development.

Furthermore, it has been shown that L1 is necessary for the maintenance of indeterminacy in the underlying meristem layers (Kessler et al., 2006). To investigate the effects of L1 on compound leaf development, different genes driven by the *UOF1* promoter were transformed into mutant or wild-type plants. The *proUOF1:SGL1* cannot rescue the leaf defect of the *sgl1-1* mutant (Figure 9D; Supplemental Figure 13, A and C), indicating that L1-specific expression of *SGL1* did not sufficient for proper compound leaf development. *KNOXI* genes were essential for the regulation of indeterminacy of SAM, and overexpression of *SHOOTMERISTEMLESS* (*STM*)/*BREVIPEDICELLUS* (*BP*)-like *MtKNOXI* genes increased leaf complexity by producing ectopic leaflets along the petiolules in *M. truncatula* (Figure 9E; Supplemental Figure 13, B and C; Zhou et al., 2014). To explore whether the L1-specific expression of *MtKNOXI* was able to form ectopic leaflets, the *proUOF1:MtKNOX2* construction was introduced into wild-type plants. The transgenic plants showed the normal compound leaf patterning (Figure 9F; Supplemental Figure 13, B and C), suggesting that increased *MtKNOX2* activity in L1 did not alter the indeterminacy during leaf development. These data indicate that *SGL1* and *MtKNOXI* in L1 play limited roles in the regulation of the indeterminacy during leaf formation.

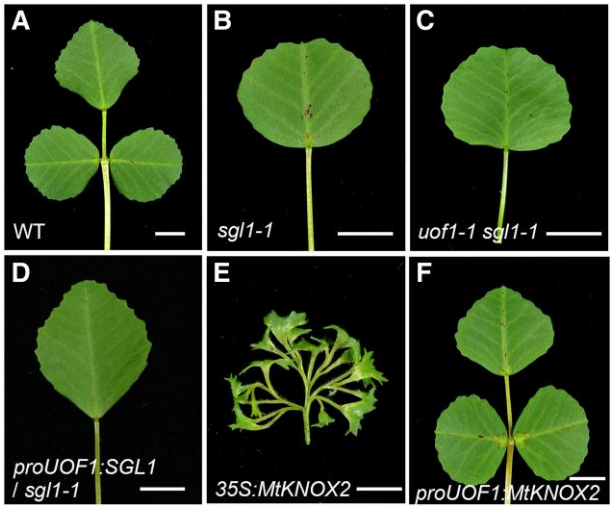

Figure 9 The function of the L1 in compound leaf patterning. Leaves of wild-type (A), *sgl1-1* (B), *uof1-1 sgl1-1* (C), *proUOF1:SGL1*/*sgl1-1* (D), *35S:MtKNOX2* (E), and *proUOF1:MtKNOX2* (F). Bars, 5 mm in (A–F).

Discussion

The roles of *UOF1* and *UOF2* genes in cuticle formation and organ development

In plants, the outer epidermal cells and cuticle present a barrier that maintains the external integrity of the plant (Samuels et al., 2008; Yeats and Rose, 2013). The plant cuticle is composed of lipophilic polymer cutin and cuticular waxes, which are synthesized from long-chain fatty acids, C16 or C18 fatty acids (Lee and Suh, 2013; Fich et al., 2016). The synthesized fatty acids are further elongated into VLCFAs. VLCFAs are major components of cuticular waxes, seed storage triacylglycerols, sphingolipids, suberin, and ω-hydroxylated fatty acids which involve in cutin monomer synthesis (Becraft, 1999; Pollard et al., 2008; Kunst and Samuels, 2009; Dominguez et al., 2011; Bernard and Joubes, 2013). In this study, the total amount of wax of both *uof1* and *uof2* mutants was significantly decreased, indicating that *UOF1* and *UOF2* play a similar role in the formation of the cuticle. It is notable that the amount of cutin was slightly increased in *uof1-1* and *uof2-1* mutants. The possible reason is that the blocked wax biosynthesis may lead to more C16 or C18 fatty acid precursors which subsequently participate in the cutin biosynthesis pathway.

The cuticle plays an important role in defining organ boundaries and allows organs to fully separate from each other

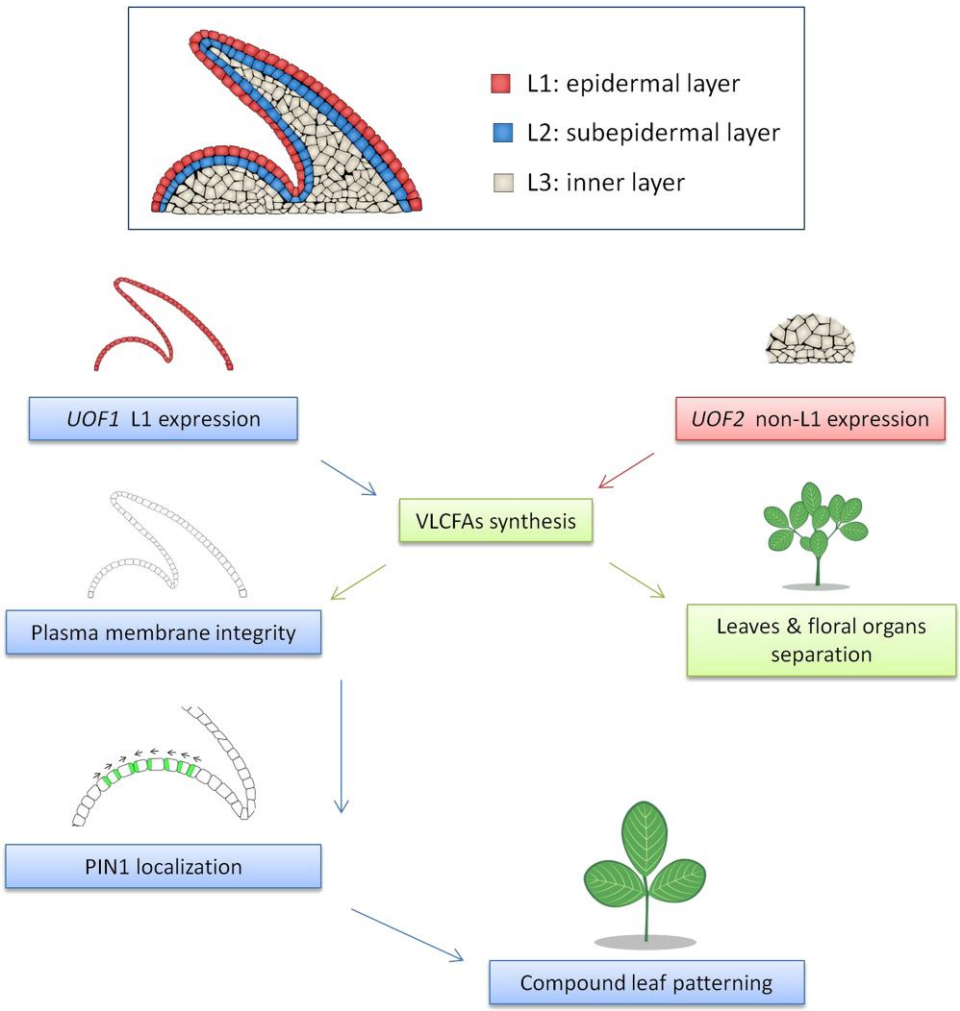

Figure 10 A proposed model of very long-chain fatty acids (VLCFAs) involved compound leaf patterning formation in *M. truncatula*. The shoot apical meristem (SAM) is divided into three distinct cell layers called L1/epidermal, L2/subepidermal, and L3/inner cell layer. Both *UOF1* and *UOF2* encode enzymes involved in the synthesis of VLCFAs, which is required for proper epidermal cuticular wax deposition, and loss of *UOF1* and *UOF2* function lead to cuticular wax-dependent organ adhesions between flowers and leaves. The *UOF1* gene is specifically expressed in the L1 of the SAM and developing leaf primordia, whereas the *UOF2* gene shows a non-L1-specific expression pattern. Furthermore, the L1-specific VLCFAs are also essential for the integrity of the plasma membrane, which is associated with the correct polar localization of PIN1 ortholog SLM1 during compound leaf patterning formation.

during organogenesis (Fich et al., 2016). Thus, structural integrity of the cuticle is necessary to prevent organ fusion. In *Arabidopsis*, the LACERATA (LCR) enzyme CYP86A8, the BAHD family acyltransferase DCR, and the FAD-containing oxidoreductase HTH are required for cutin biosynthesis. Loss-of-function mutants of these genes display defective cuticle and exhibit strong fusion between rosette leaves and inflorescences (Wellesen et al., 2001; Krolikowski et al., 2003; Panikashvili et al., 2009). *FDH*, *ONI1*, and *ECERIFERUM10* (*CER10*) encode FAE that involved in the synthesis of cuticular waxes, and their mutants show a strong organ fusion in leaves (Yephremov et al., 1999; Zheng et al., 2005; Ito et al., 2011). Furthermore, Arabidopsis *CER8* encodes LACS1 that has overlapping functions with LACS2 in wax and cutin synthesis, and the *lacs1 lacs2* double mutants display organ fusion between leaves (Lu et al., 2009; Weng et al., 2010). Expression of WAX INDUCER1 (WIN1) chimeric repressor (*35S:WIN1-SRDX*) also severely impaired the cuticular wax and cutin composition, which leads to adhesions between leaves and buds (Oshima et al., 2013). In *M. truncatula*, mutation of both *UOF1* and *UOF2* results in plants with organ adhesions between flowers and leaves. These findings indicate that the organ fusion is a typical characteristic of cuticle mutants among species.

Previous studies showed that the changes in composition and content of wax and cutin have effects on leaf size. In Arabidopsis, *GROW FAST ON CYTOKININS1* (*GFC1*) and *DESPERADO* (*DSO*) encode enzyme and transporter that involved in cutin synthesis and secretion (Panikashvili et al., 2007; Wu et al., 2015). The *gfc1* mutants produce larger leaves, while the *dso* mutant develop smaller leaves. In rice,

the leaves of *oni3* mutant and the *curly flag leaf1* (*cfl1*) dominant mutant are covered with less wax, and show a shortened and curled leaf phenotype, respectively (Wu et al., 2011; Akiba et al., 2014). Moreover, the leaf margin formation was affected in these kinds of mutants. *BDG* encodes a cell wall localized α/β-hydrolase fold protein and participates in cutin synthesis (Kurdyukov et al., 2006). The *bdg* mutants produce elongated leaves with a smooth margin. In this study, the smooth leaf margin was also produced in *uof1* mutant, instead of *uof2* mutant, indicating that the specific expression of *UOF1* in leaf margin is involved in the marginal serration formation. To our surprise, *uof1* mutants showed increased leaflet number, which is different from the previous reports in other compound-leafed species. For example, *stkcs6*, the mutant of wax synthesis in potato (*Solanum tuberosum* L.), and *cutin deficient2*, the mutant of cutin synthesis in tomato (*Solanum lycopersicum*) did not show the defects in the compound leaf pattern (Serra et al., 2009; Nadakuduti et al., 2012; Kimbara et al., 2013). These findings suggest that *UOF1* may play a species-specific function in leaf patterning in *M. truncatula* (Figure 10).

UOF1-dependent VLCFAs synthesis is critical for L1 integrity

The epidermis is formed by the L1 in the SAM and plays a critical role in the establishment and maintenance of the plant body (Yadav et al., 2014; Shapiro et al., 2015). The mutants with defects in L1 cell specification exhibited disorganized morphology (Ingram, 2007; Savaldi-Goldstein and Chory, 2008). *FDH* and *ONI1* are specifically expressed in L1 and control epidermis identification in Arabidopsis and rice (Yephremov et al., 1999; Ito et al., 2011). Two receptor-like protein kinases, the *Arabidopsis thaliana* homolog of *CRINKLY4* (*ACR4*) and *ABNORMAL LEAF SHAPE2* (*ALE2*), are also specifically expressed in L1 and necessary for the proper differentiation of epidermal cells by regulating the expression of *FDH* in *A. thaliana* (Watanabe et al., 2004; Tanaka et al., 2007). Moreover, the integrity of L1 cells is affected by the biosynthesis of membrane lipids. In plants, phosphatidylcholine is a major lipid component in cell membranes, accounting for up to 60% of total membrane lipids (Moreau et al., 1998). The main step in phosphatidylcholine biosynthesis is the triple, sequential *N*-methylation of phosphoethanolamine, catalyzed by *S*-adenosyl-L-methionine:phosphoethanolamine *N*-methyltransferase (PEAMT) (Bolognese and McGraw, 2000; McNeil et al., 2000). Mutation in *PEAMT* changes the root epidermal cell integrity and root architecture (Cruz-Ramírez et al., 2004). In this study, *UOF1* is specifically expressed in L1, which is confirmed by RNA in situ hybridization and promoter-GFP reporter plants. Additionally, the analysis of plasma membrane by observation of the *35S:AtPIP2A-GFP* showed that loss of *UOF1* function causes the defects in membrane integrity in L1. Therefore, these observations demonstrate a link between VLCFAs biosynthesis and the proper development of L1 in *M. truncatula* (Figure 10).

UOF1 regulates compound leaf patterning formation by modulating the polarity localization of AtPIN1/SLM1

The plant hormone auxin is an important regulator of plant growth and development (Benjamins and Scheres, 2008). Auxin is known to regulate the initiation of leaf primordia from the SAM, and the formation of leaf serrations (Benková et al., 2003; Barkoulas et al., 2008; Koenig et al., 2009). Directional auxin transport in the L1 of SAM is mainly mediated by the polar distribution of PIN1 (Leyser, 2011; Band et al., 2014; Adamowski and Friml, 2015). The polar localization of PIN1 can be modified by several factors, including the Ser/Thr protein kinase PINOID (PID), the fatty acids composition of the L1 plasma membrane, and protein-mediated subcellular trafficking and redirection (Christensen et al., 2000; Friml et al., 2004; Huang et al., 2010; Marhava, 2022). PID activates auxin efflux through phosphorylation of the four serines S1–S4 at PIN1, and acts as a binary switch in the apical-basal polar targeting of PIN proteins (Christensen et al., 2000; Luschnig and Vert, 2014). PINs cycle between their plasma membrane polar domains and endosomal compartments in a continuous and dynamic manner, and several components, such as cytoskeletal components and membrane lipid composition, are involved in this delivery (Kleine-Vehn et al., 2008; Naramoto, 2017; Sauer and Kleine-Vehn, 2019). Mutants with defects in fatty acids and their derivatives, such as sterols, sphingolipids, and phosphatidylcholine, showed disturbed cell polarity, PIN protein positioning, and auxin distribution (Prud'homme and Moore, 1992). A mutation in the *CEPHALOPOD* (*CPH*), also referred to as *SMT1*, results in a significant decrease in the level of sitosterol and an increase in the level of cholesterol, leading to conspicuous cell polarity defects and redistribution of PIN1 protein in membranes of elongated vascular cells (Willemsen, 2003). In *M. truncatula*, both leaf margin formation and compound leaf development are cooperatively regulated by the auxin/SLM1 module (Zhou et al., 2011, 2013). Accordingly, *uof1* mutant also displayed the similar defects, which are relatively smooth leaf margin and altered compound leaf patterning. We demonstrate that *UOF1* is involved in the leaf patterning formation by regulating L1 plasma membrane integrity and subsequent polar distribution of PIN1. Taken together, these observations provide evidence that *UOF1*-mediated biosynthesis of VLCFAs in L1 play important roles in compound leaf development, which is associated with the polarization of auxin efflux carrier in *M. truncatula* (Figure 10).

L1-specific expression of *MtKNOXI* and *SGL1* play limited roles in maintaining indeterminacy of the leaf primordia

Activating indeterminacy in leaf primordia will increase leaf complexity. *KNOXI* genes play important roles in leaf development in many species (Hay and Tsiantis, 2010). In tomato and cardamine (*Cardamine hirsuta*), up-regulation of *KNOXI* genes delays leaf differentiation and prolongs the morphogenetic window, causing increased leaf complexity, indicating

that *KNOXI* genes are necessary and sufficient for leaflet formation (Hay and Tsiantis, 2006; Shani et al., 2009). In *M. truncatula*, ectopic expression of *MtKNOXI* genes is sufficient for increasing the leaflet number (Zhou et al., 2014). Pea (*Pisum sativum*) *UNIFOLIATA* (*UNI*) and Medicago *SGL1* are two orthologs of Arabidopsis *LFY* gene, promoting the transient indeterminate growth of the leaf (Gourlay et al., 2000). *UNI* is expressed in the leaf blastozone, and the *uni* mutant displays reduced leaf complexity. In *M. truncatula*, *SGL1* activities are necessary for compound leaf formation (Wang et al., 2008). However, L1-specific expression of *MtKNOX2* and *SGL1* activity cannot produce ectopic leaflet and complement the defects in *sgl1* mutant, respectively, indicating that *SGL1* and *MtKNOXI* are not responsible for the compound leaf patterning in L1.

Materials and methods

Plant materials and growth conditions

The wild-type used in this study was barrelclover (*Medicago truncatula*) R108 ecotype. Mutant lines *uof1-1*, *uof1-2*, *uof1-3*, *uof1-4*, *uof2-1*, *uof2-2*, *slm1-1* (Zhou et al., 2011), and *sgl1-1* (Wang et al., 2008) were identified from the *Tnt1* retrotransposon-tagged mutant collection of *M. truncatula* R108 ecotype (Tadege et al., 2008). Scarified seeds were germinated in moist filter paper and placed at 4°C for 5 days in the dark. Plants were grown at 22°C:20°C, day:night temperatures with a 16 h:8 h, day:night photoperiod and 75% relative humidity, and 150 μmol m^{-2} s^{-1} light intensity.

Genetic complementation and promoter-GUS analysis

For genetic complementation, a 2512 and 2231 bp promoter sequence plus the genomic sequence of *UOF1* and *UOF2* were amplified using primer pairs UOF1-com-F/UOF1-com-R and UOF2-com-F/UOF2-com-R, and cloned into the gateway destination vector pEarleyGate 301. For expression pattern analysis, the 2512 and 2231 bp promoter sequences of *UOF1* and *UOF2* were amplified using primer pairs proUOF1-F/proUOF1-R and proUOF2-F/proUOF2-R, and transferred into the gateway destination vector pBGWFS7. The primers used are listed in Supplemental Table 1. All final destination vectors were introduced into the disarmed *Agrobacterium tumefaciens* EHA105 strain. For genetic complementation, leaves of *uof1-1* and *uof2-1* were transformed with EHA105 harboring *proUOF1:UOF1* and *proUOF2:UOF2* vectors, respectively. For expression pattern analysis, leaves of wild-type were transformed with *proUOF1:GUS-GFP* and *proUOF2:GUS-GFP* vectors.

RNA extraction, reverse transcription PCR (RT-PCR), and reverse transcription quantitative PCR (RT-qPCR)

To measure the transcript levels of *UOF1*, *UOF2*, and *SLM1* in wild-type and mutant plants, fully expanded leaves were harvested from wild-type and different mutant lines. To measure the tissue/organ expression patterns of *UOF1* and *UOF2*, the RNA samples were isolated from different wild-type tissues. RNA was extracted using the TRIzol reagent (Invitrogen, USA), according to the manufacturer's instructions. cDNA was synthesized with 2 μg of total RNA using the PrimeScript II cDNA Synthesis Kit (Takara, Japan). The cDNA was used as templates for RT-PCR and RT-qPCR. RT-qPCR was performed using the SYB RT-qPCR mix (TaKaRa, Japan), and three biological samples were repeated. The $2^{-\Delta\Delta CT}$ method was used to calculate relative expression levels, respectively. The *MtActin* gene was used as an internal control (Livak and Schmittgen, 2001). The primers used for RT-PCR and RT-qPCR analysis are listed in Supplemental Table 1.

RNA in situ hybridization

For RNA in situ hybridization, the probe fragments of 450 bp *UOF1* CDS, 380 bp *UOF2* CDS, and 553 bp *SLM1* CDS were polymerase chain reaction amplified using primers listed in Supplemental Table 1. These PCR products were cloned into pGEM-T vector (Promega, USA) and then labeled with digoxigenin-11-UTP (Roche, Switzerland). RNA in situ hybridization was performed on vegetative and reproductive shoot buds of wild-type or *uof1-1* plants as described previously (Zhou et al., 2011). The results were visualized using a fluorescence microscope (Olympus, Japan).

Sequences alignment and phylogenetic analysis

For sequences alignment, the full-length protein sequences of the KCS and CYP86A family members from *M. truncatula* and Arabidopsis (*Arabidopsis thaliana*) were aligned using online CLUSTALW (http://www.genome.jp/tools/clustalw/). The phylogenetic trees of the KCS and CYP86A family members were constructed using MEGA6 software suite (http://www.megasoftware.net/) by the Neighbor-Joining (NJ) method with 1000 bootstrap replicates in the p-distance model.

Scanning electron microscopy (SEM) analysis and toluidine blue (TB) staining

For SEM analysis, the leaves, flowers, pods, and reproductive shoot buds were fixed in 3% (v/v) glutaraldehyde, washed five times in 1 × PBS every 30 min, dehydrated in a series of ethanol (30%, 50%, 60%, 70%, 85%, 95%, 100% [v/v]) every 30 min, and then carbon dioxide dried and sprayed with gold powder. The samples were viewed under a Tecnai electron microscope (FEI, USA) using an accelerating voltage of 10 kV. The TB staining protocol was followed as described previously (Tanaka et al., 2004). Briefly, an aqueous solution of 0.05% (w/v) TB (Sigma, USA) was poured onto the plates on which samples were submerged. After 10 min, the TB solution was removed, and the leaves and flowers were washed with water.

Pollen staining and β-glucuronidase (GUS) staining

To determine pollen viability, flowers of the wild-type, *uof1-1*, and *uof2-1* were collected and fixed by Carnoy's fixative for 2 h at room temperature, and then stained with Alexander's solution for 2 h at room temperature as described (Alexander, 1969). For GUS staining, flowers and fully expanded leaves were collected. The GUS activity was histochemically detected as previously described (Jefferson et al., 1987).

GFP fluorescence imaging

The marker lines, *proAtPIN1:AtPIN1-GFP*/WT (Zhou et al., 2011) and *proAtPIP2A-GFP*/WT (Luo and Nakata, 2012), were obtained as described. For fluorescent analysis of *proAtPIN1:AtPIN1-GFP* and *proAtPIP2A-GFP* in wilt-type and *uof1-1* plants. The marker plants were crossed with *uof1-1* (+/−), respectively, and then selfed to generate the *proAtPIN1:AtPIN1-GFP/uof1-1* (−/−) and *proAtPIP2A-GFP/uof1-1* (−/−) plants. Apical shoot buds and leaves were collected and observed with a Zeiss 780 confocal laser scanning microscope (Zeiss, Germany). The GFP signals were excited at 488 nm line of an argon laser, and emission was collected at 510 nm. All experiments are representative of at least 10 observed samples from three independent experiments.

Cuticular waxes and cutin analysis

The cuticular waxes and cutin composition of 4-week-old leaves of wild-type, *uof1-1*, and *uof2-1* were determined as described (Lu et al., 2011). For identification of monounsaturated primary alcohols, thin layer chromatography (TLC) analysis was used to purify the primary alcohols. The total wax mixtures from leaves of wild-type, *uof1-1*, and *uof2-1* were separated on silica gel plates using hexane-diethylether-acetic acid (50:50:1 [v/v/v]) (Sigma-Aldrich, USA). The alcohol fraction was scraped off and extracted in chloroform, dried under nitrogen, and derivatized with *N*,*O*-bis(trimethylsilyl)trifluoroacetamide (BSTFA) (Sigma-Aldrich, USA), then analyzed on gas chromatography-flame ionization detector (GC-FID) and gas chromatography-mass spectrometer (GC-MS). To determine the location of the double bond, the monounsaturated fatty alcohols were first converted to acetic ester by acetic anhydride and then derivatized by dimethyl disulfide (DMDS) (Sigma-Aldrich, USA), and finally analyzed by GC-MS using the method as described (Leonhardt and Devilbiss, 1985).

Transcriptomic assay

For transcriptomic analysis, shoot buds were harvested from 4-week-old wild-type and *uof1-1* mutant plants. Three biological replicates of each sample were prepared. The total RNA of each sample was extracted, and all samples were sequenced on a BGISEQ-500 platform at the BGI Genomics Institute (BGI-Shenzhen, China). For each replicate, RNA sequencing generated more than 20 million raw reads. Raw reads were first purified by Trimmomatic (v0.37, BGI-Shenzhen, China) (Chen et al., 2018). Adapter sequences, low-quality reads, and reads containing more than 5% unknown nucleotides were filtered out from raw reads. Then, clean reads were aligned against the annotated *M. truncatula* reference transcriptome using Bowtie (v4.0, Baltimore, USA). RSEM (RNA-Seq by Expectation Maximization) was used for gene expression analysis and R package DEGseq (Differentially Expressed Gene Identification for RNA-seq data) was used for identifying DEGs. All DEGs characterized were up-/down-regulated more than two-fold and had a false discovery rate (FDR) < 0.001. The hypergeometric test of *P*-value adjusted by the FDR method was used to evaluate the enrichment of GO terms and the KEGG pathway. The heatmap was created by Helm software (Heatmap Illustrator, version 1.0). The DEGs are listed in Supplemental Table 2.

Measurements of free IAA contents

For quantification of free IAA content, the leaves from 4-week-old wild-type and *uof1-1* mutants were harvested and weighed (each sample 200 mg), and then ground into powder in liquid nitrogen. Add 1 ml ethyl acetate, containing 200 ng ^{15}N-IAA served as an internal standard, to the samples and then vortexed for 10 min. After centrifugation at 15,000*g* for 10 min at 4°C, the supernatants were collected and the pellets were re-extracted with 0.5 ml ethyl acetate. The combined supernatants were evaporated to dryness in a vacuum concentrator. The acquired residues were resuspended in 0.5 ml of 70% (v/v) methanol, and then supernatants were pipetted to glass vials for high performance liquid chromatography-tandem mass spectrometry (HPLC-MS/MS) analysis (Prominence LC-20A and LCMS-8040; Shimadzu, Kyoto, Japan).

Measurement of water loss

For water loss rate analysis, 4-week-old leaves from wild-type, *uof1-1*, and *uof2-1* plants were collected and maintained at room temperature. Weight was measured at different time points. Then the leaves were put in a 60°C oven overnight. Total water was defined as the fresh weight less the dry weight after the heat treatment. The water loss at each time point was expressed as the percentage of the water loss over total water.

Statistical analysis

Error bars in RT-qPCR, free IAA content, water loss, and wax and cutin measurement figures show the standard deviation of three biological replicates, as indicated in the legends. Most of the pairwise comparisons between the means were performed using a two-sided Student's *t* test, using GraphPad Prism version 9 software.

Data availability

The data used to support the findings of this study appeared in the article and are available from the corresponding author.

Accession numbers

Sequence data from this article can be found in the *Medicago truncatula* R108_HiC website (https://medicago.toulouse.inrae.fr/MtrunR108_HiC/): UOF1, Medtr3g105550; UOF2, Medtr8g030590; SLM1, Medtr7g089360; SGL1, Medtr3g098560; MtKNOX2, Medtr1g017080.

Supplemental data

The following materials are available in the online version of this article.

Supplemental Figure S1. SEM analysis and pollen staining of flower organs of wild-type, *uof1-1*, and *uof2-1* mutants.

Supplemental Figure S2. Genetic segregation ratio and co-segregation analysis of *uof1* and *uof2* mutants.

Supplemental Figure S3. Phylogenetic analysis of the KCS family proteins in *A. thaliana* (At) and *M. truncatula* (Mt).

Supplemental Figure S4. Alignment of amino acid sequences of UOF1 and its homologs from different species.

Supplemental Figure S5. Phylogenetic analysis of the cytochrome P450 CYP86 subfamily proteins in *A. thaliana* (At) and *M. truncatula* (Mt).

Supplemental Figure S6. Alignment of amino acid sequences of UOF2 and its homologs from different species.

Supplemental Figure S7. Organ adhesion phenotypes of *uof1* and *uof2* mutants.

Supplemental Figure S8. Leaves and flowers phenotype of the single and double mutants and genetic complementation analysis.

Supplemental Figure S9. The expression pattern of *UOF1*.

Supplemental Figure S10. Comparison of functional categories of differentially expressed genes in *uof1-1* and wild-type shoot buds.

Supplemental Figure S11. SEM images of epidermal cells of wild-type and *uof1-1* leaves.

Supplemental Figure S12. Leaf and cuticle wax phenotype of the *uof1-1 slm1-1* double mutants.

Supplemental Figure S13. The function of *UOF1* in compound leaf patterning.

Supplemental Table S1. Primers used in this study.

Supplemental Table S2. The differentially expressed genes (DEGs) in WT and *uof1-1* mutant shoot buds.

Acknowledgments

We thank Dr Sen Wang from the State Key Laboratory of Microbial Technology, Shandong University for the assistance in SEM analysis.

Funding

This work was supported by grants from the National Natural Science Foundation of China (31871459, 31900172, and 32201446), the Natural Science Foundation of Shandong Province (ZR2020KC018 and ZR2021QC032), and the China Postdoctoral Science Foundation (2021M691948). Development of *M. truncatula Tnt1* mutant population was, in part, funded by the National Science Foundation, USA (DBI-0703285 and IOS-1127155).

Conflict of interest statement: The authors have no conflicts of interest to declare.

References

Adamowski M, Friml J (2015) PIN-dependent auxin transport: action, regulation, and evolution. Plant Cell **27**(1): 20–32

Akiba T, Hibara K, Kimura F, Tsuda K, Shibata K, Ishibashi M, Moriya C, Nakagawa K, Kurata N, Itoh J, et al. (2014) Organ fusion and defective shoot development in *oni3* mutants of rice. Plant Cell Physiol **55**(1): 42–51

Alexander MP (1969) Differential staining of aborted and nonaborted pollen. Stain Technol **44**(3): 117–125

Band LR, Wells DM, Fozard JA, Ghetiu T, French AP, Pound MP, Wilson MH, Yu L, Li W, Hijazi HI, et al. (2014) Systems analysis of auxin transport in the *Arabidopsis* root apex. Plant Cell **26**(3): 862–875

Barkoulas M, Hay A, Kougioumoutzi E, Tsiantis M (2008) A developmental framework for dissected leaf formation in the *Arabidopsis* relative *Cardamine hirsuta*. Nat Genet **40**(9): 1136–1141

Barton MK (2010) Twenty years on: the inner workings of the shoot apical meristem, a developmental dynamo. Dev Biol **341**(1): 95–113

Becraft PW (1999) Development of the leaf epidermis. Curr Top Dev Biol **45**(C): 1–40

Benjamins R, Scheres B (2008) Auxin: the looping star in plant development. Annu Rev Plant Biol **59**(1): 443–465

Benková E, Michniewicz M, Sauer M, Teichmann T, Seifertová D, Jürgens G, Friml J (2003) Local, efflux-dependent auxin gradients as a common module for plant organ formation. Cell **115**(5): 591–602

Bernard A, Joubes J (2013) Arabidopsis cuticular waxes: advances in synthesis, export and regulation. Prog Lipid Res **52**(1): 110–129

Bessire M, Borel S, Fabre G, Carraca L, Efremova N, Yephremov A, Cao Y, Jetter R, Jacquat AC, Metraux JP, et al. (2011) A member of the PLEIOTROPIC DRUG RESISTANCE family of ATP binding cassette transporters is required for the formation of a functional cuticle in *Arabidopsis*. Plant Cell **23**(5): 1958–1970

Bird D, Beisson F, Brigham A, Shin J, Greer S, Jetter R, Kunst L, Wu X, Yephremov A, Samuels L (2007) Characterization of *Arabidopsis* ABCG11/WBC11, an ATP binding cassette (ABC) transporter that is required for cuticular lipid secretion. Plant J **52**(3): 485–498

Bolognese CP, McGraw P (2000) The isolation and characterization in yeast of a gene for *Arabidopsis S*-adenosylmethionine:phospho-ethanolamine *N*-methyltransferase. Plant Physiol **124**(4): 1800–1813

Byrt CS, Zhao MC, Kourghi M, Bose J, Henderson SW, Qiu JE, Gilliham M, Schultz C, Schwarz M, Ramesh SA, et al. (2017) Non-selective cation channel activity of aquaporin AtPIP2;1 regulated by Ca^{2+} and pH. Plant Cell Environ **40**(6): 802–815

Champagne CE, Goliber TE, Wojciechowski MF, Mei RW, Townsley BT, Wang K, Paz MM, Geeta R, Sinha NR (2007) Compound leaf development and evolution in the legumes. Plant Cell **19**(11): 3369–3378

Chen Y, Chen Y, Shi C, Huang Z, Zhang Y, Li S, Li Y, Ye J, Yu C, Li Z, et al. (2018) SOAPnuke: a MapReduce acceleration-supported software for integrated quality control and preprocessing of high-throughput sequencing data. Gigascience **7**(1): 1–6

Christensen SK, Dagenais N, Chory J, Weigel D (2000) Regulation of auxin response by the protein kinase PINOID. Cell **100**(4): 469–478

Cruz-Ramírez A, López-Bucio J, Ramírez-Pimentel G, Zurita-Silva A, Sánchez-Calderon L, Ramírez-Chávez E, González-Ortega E, Herrera-Estrella L (2004) The *xipotl* mutant of *Arabidopsis* reveals

a critical role for phospholipid metabolism in root system development and epidermal cell integrity. Plant Cell **16**(8): 2020–2034

de Reuille PB, Bohn-Courseau I, Ljung K, Morin H, Carraro N, Godin C, Traas J (2006) Computer simulations reveal properties of the cell-cell signaling network at the shoot apex in *Arabidopsis*. Proc Natl Acad Sci U S A **103**(5): 1627–1632

Debono A, Yeats TH, Rose JK, Bird D, Jetter R, Kunst L, Samuels L (2009) *Arabidopsis* LTPG is a glycosylphosphatidylinositol-anchored lipid transfer protein required for export of lipids to the plant surface. Plant Cell **21**(4): 1230–1238

Diener AC, Li H, Zhou W, Whoriskey WJ, Nes WD, Fink GR (2000) *Sterol methyltransferase 1* controls the level of cholesterol in plants. Plant Cell **12**(6): 853–870

Dominguez E, Heredia-Guerrero JA, Heredia A (2011) The biophysical design of plant cuticles: an overview. New Phytol **189**(4): 938–949

Efremova N, Schreiber L, Bar S, Heidmann I, Huijser P, Wellesen K, Schwarz-Sommer Z, Saedler H, Yephremov A (2004) Functional conservation and maintenance of expression pattern of *FIDDLEHEAD*-like genes in *Arabidopsis* and *Antirrhinum*. Plant Mol Biol **56**(5): 821–837

Fich EA, Segerson NA, Rose JK (2016) The plant polyester cutin: biosynthesis, structure, and biological roles. Annu Rev Plant Biol **67**(1): 207–233

Friml J, Yang X, Michniewicz M, Weijers D, Quint A, Tietz O, Benjamins R, Ouwerkerk PBF, Ljung K, Sandberg G, et al. (2004) A PINOID-dependent binary switch in apical-basal PIN polar targeting directs auxin efflux. Science **306**(5697): 862–865

Furner I J, Pumfrey JE (1992) Cell fate in the shoot apical meristem of *Arabidopsis thaliana*. Development **115**(3): 755–764

Gourlay CW, Hofer JM, Ellis TH (2000) Pea compound leaf architecture is regulated by interactions among the genes *UNIFOLIATA*, *COCHLEATA*, *AFILA*, and *TENDRIL-LESS*. Plant Cell **12**(8): 1279–1294

Hay A, Tsiantis M (2006) The genetic basis for differences in leaf form between *Arabidopsis thaliana* and its wild relative *Cardamine hirsuta*. Nat Genet **38**(8): 942–947

Hay A, Tsiantis M (2010) KNOX Genes: versatile regulators of plant development and diversity. Development **137**(19): 3153–3165

Hegebarth D, Jetter R (2017) Cuticular waxes of *Arabidopsis thaliana* shoots: cell-type-specific composition and biosynthesis. Plants (Basel) **6**(4): 27

Heisler MG, Ohno C, Das P, Sieber P, Reddy GV, Long JA, Meyerowitz EM (2005) Patterns of auxin transport and gene expression during primordium development revealed by live imaging of the *Arabidopsis* inflorescence meristem. Curr Biol **15**(21): 1899–1911

Huang F, Zago MK, Abas L, van Marion A, Galvan-Ampudia CS, Offringa R (2010) Phosphorylation of conserved PIN motifs directs *Arabidopsis* PIN1 polarity and auxin transport. Plant Cell **22**(4): 1129–1142

Ingram GC (2007) Signalling during epidermal development. Biochem Soc Trans **35**(1): 156–160

Ito Y, Kimura F, Hirakata K, Tsuda K, Takasugi T, Eiguchi M, Nakagawa K, Kurata N (2011) Fatty acid elongase is required for shoot development in rice. Plant J **66**(4): 680–688

Jefferson RA, Kavanagh TA, Bevan MW (1987) GUS Fusions: beta-glucuronidase as a sensitive and versatile gene fusion marker in higher plants. EMBO J **6**(13): 3901–3907

Joubes J, Raffaele S, Bourdenx B, Garcia C, Laroche-Traineau J, Moreau P, Domergue F, Lessire R (2008) The VLCFA elongase gene family in *Arabidopsis thaliana*: phylogenetic analysis, 3D modelling and expression profiling. Plant Mol Biol **67**(5): 547–566

Kessler S, Townsley B, Sinha N (2006) L1 division and differentiation patterns influence shoot apical meristem maintenance. Plant Physiol **141**(4): 1349–1362

Kim H, Lee SB, Kim HJ, Min MK, Hwang I, Suh MC (2012) Characterization of glycosylphosphatidylinositol-anchored lipid transfer protein 2 (LTPG2) and overlapping function between LTPG/LTPG1 and LTPG2 in cuticular wax export or accumulation in *Arabidopsis thaliana*. Plant Cell Physiol **53**(8): 1391–1403

Kimbara J, Yoshida M, Ito H, Kitagawa M, Takada W, Hayashi K, Shibutani Y, Kusano M, Okazaki Y, Nakabayashi R, et al. (2013) Inhibition of *CUTIN DEFICIENT 2* causes defects in cuticle function and structure and metabolite changes in tomato fruit. Plant Cell Physiol **54**(9): 1535–1548

Kleine-Vehn J, Dhonukshe P, Sauer M, Brewer PB, Wiśniewska J, Paciorek T, Benková E, Friml J (2008) ARF GEF-dependent transcytosis and polar delivery of PIN auxin carriers in *Arabidopsis*. Curr Biol **18**(7): 526–531

Koenig D, Bayer E, Kang J, Kuhlemeier C, Sinha N (2009) Auxin patterns *Solanum lycopersicum* leaf morphogenesis. Development **136-**(17): 2997–3006

Krolikowski KA, Victor JL, Wagler TN, Lolle SJ, Pruitt RE (2003) Isolation and characterization of the *Arabidopsis* organ fusion gene *HOTHEAD*. Plant J **35**(4): 501–511

Kunst L, Samuels L (2009) Plant cuticles shine: advances in wax biosynthesis and export. Curr Opin Plant Biol **12**(6): 721–727

Kurdyukov S, Faust A, Nawrath C, Bar S, Voisin D, Efremova N, Franke R, Schreiber L, Saedler H, Metraux JP, et al. (2006) The epidermis-specific extracellular BODYGUARD controls cuticle development and morphogenesis in *Arabidopsis*. Plant Cell **18**(2): 321–339

Lee SB, Suh MC (2013) Recent advances in cuticular wax biosynthesis and its regulation in *Arabidopsis*. Mol Plant **6**(2): 246–249

Leonhardt BA, Devilbiss ED (1985) Separation and double-bond determination on nanogram quantities of aliphatic monounsaturated alcohols, aldehydes and carboxylic-acid methyl-esters. J Chromatogr **322**(C): 484–490

Leyser O (2011) Auxin, self-organisation, and the colonial nature of plants. Curr Biol **21**(9): R331–R337

Li-Beisson Y, Pollard M, Sauveplane V, Pinot F, Ohlrogge J, Beisson F (2009) Nanoridges that characterize the surface morphology of flowers require the synthesis of cutin polyester. Proc Natl Acad Sci U S A **106**(51): 22008–22013

Li-Beisson Y, Shorrosh B, Beisson F, Andersson MX, Arondel V, Bates PD, Baud S, Bird D, Debono A, Durrett TP, et al. (2013) Acyl-lipid metabolism. Arabidopsis Book **11**: e0161

Livak KJ, Schmittgen TD (2001) Analysis of relative gene expression data using real-time quantitative PCR and the $2^{-\Delta\Delta CT}$ method. Methods **25**(4): 402–408

Lolle SJ, Cheung AY, Sussex IM (1992) *Fiddlehead*—an *Arabidopsis* mutant constitutively expressing an organ fusion program that involves interactions between epidermal-cells. Dev Biol **152**(2): 383–392

Lolle SJ, Pruitt RE (1999) Epidermal cell interactions: a case for local talk. Trends Plant Sci **4**(1): 14–20

Lu S, Song T, Kosma DK, Parsons EP, Rowland O, Jenks MA (2009) Arabidopsis *CER8* encodes LONG-CHAIN ACYL-COA SYNTHETASE 1 (LACS1) that has overlapping functions with LACS2 in plant wax and cutin synthesis. Plant J **59**(4): 553–564

Lu SY, Zhao HY, Parsons EP, Xu CC, Kosma DK, Xu XJ, Chao D, Lohrey G, Bangarusamy DK, Wang G, et al. (2011) The *glossyhead1* allele of *ACC1* reveals a principal role for multidomain acetyl-coenzyme A carboxylase in the biosynthesis of cuticular waxes by Arabidopsis. Plant Physiol **157**(3): 1079–1092

Luo B, Nakata PA (2012) A set of GFP organelle marker lines for intracellular localization studies in *Medicago truncatula*. Plant Sci **188-189**: 19–24

Luschnig C, Vert G (2014) The dynamics of plant plasma membrane proteins: PINs and beyond. Development **141**(15): 2924–2938

Marhava P (2022) Recent developments in the understanding of PIN polarity. New Phytol **233**(2): 624–630

McNeil SD, Nuccio ML, Rhodes D, Shachar-Hill Y, Hanson AD (2000) Radiotracer and computer modeling evidence that phospho-base methylation is the main route of choline synthesis in tobacco. Plant Physiol **123**(1): 371–380

Millar AA, Kunst L (1997) Very-long-chain fatty acid biosynthesis is controlled through the expression and specificity of the condensing enzyme. Plant J **12**(1): 121–131

Moreau P, Bessoule JJ, Mongrand S, Testet E, Vincent P, Cassagne C (1998) Lipid trafficking in plant cells. Prog Lipid Res **37**(6): 371–391

Nadakuduti SS, Pollard M, Kosma DK, Allen C Jr, Ohlrogge JB, Barry CS (2012) Pleiotropic phenotypes of the *sticky peel* mutant provide new insight into the role of *CUTIN DEFICIENT2* in epidermal cell function in tomato. Plant Physiol **159**(3): 945–960

Naramoto S (2017) Polar transport in plants mediated by membrane transporters: focus on mechanisms of polar auxin transport. Curr Opin Plant Biol **40**: 8–14

Oshima Y, Shikata M, Koyama T, Ohtsubo N, Mitsuda N, Ohme-Takagi M (2013) MIXTA-like transcription factors and WAX INDUCER1/SHINE1 coordinately regulate cuticle development in *Arabidopsis* and *Torenia fournieri*. Plant Cell **25**(5): 1609–1624

Panikashvili D, Savaldi-Goldstein S, Mandel T, Yifhar T, Franke RB, Höfer R, Schreiber L, Chory J, Aharoni A (2007) The Arabidopsis DESPERADO/AtWBC11 transporter is required for cutin and wax secretion. Plant Physiol **145**(4): 1345–1360

Panikashvili D, Shi JX, Schreiber L, Aharoni A (2009) The Arabidopsis *DCR* encoding a soluble BAHD acyltransferase is required for cutin polyester formation and seed hydration properties. Plant Physiol **151**(4): 1773–1789

Panikashvili D, Shi JX, Schreiber L, Aharoni A (2011) The Arabidopsis ABCG13 transporter is required for flower cuticle secretion and patterning of the petal epidermis. New Phytol **190**(1): 113–124

Perales M, Reddy GV (2012) Stem cell maintenance in shoot apical meristems. Curr Opin Plant Biol **15**(1): 10–16

Pollard M, Beisson F, Li YH, Ohlrogge JB (2008) Building lipid barriers: biosynthesis of cutin and suberin. Trends Plant Sci **13**(5): 236–246

PostBeittenmiller D (1996) Biochemistry and molecular biology of wax production in plants. Annu Rev Plant Physiol Plant Mol Biol **47**(1): 405–430

Prud'homme MP, Moore TS (1992) Phosphatidylcholine synthesis in castor bean endosperm: occurrence of an *S*-adenosyl-L-methionine:ethanolamine *N*-methyltransferase. Plant Physiol **100**(3): 1536–1540

Pruitt RE, Vielle-Calzada JP, Ploense SE, Grossniklaus U, Lolle SJ (2000) *FIDDLEHEAD*, a gene required to suppress epidermal cell interactions in *Arabidopsis*, encodes a putative lipid biosynthetic enzyme. Proc Natl Acad Sci U S A **97**(3): 1311–1316

Pulsifer IP, Kluge S, Rowland O (2012) Arabidopsis LONG-CHAIN ACYL-COA SYNTHETASE 1 (LACS1), LACS2, and LACS3 facilitate fatty acid uptake in yeast. Plant Physiol Biochem **51**: 31–39

Reinhardt D, Pesce ER, Stieger P, Mandel T, Baltensperger K, Bennett M, Traas J, Friml J, Kuhlemeier C (2003) Regulation of phyllotaxis by polar auxin transport. Nature **426**(6964): 255–260

Roudier F, Gissot L, Beaudoin F, Haslam R, Michaelson L, Marion J, Molino D, Lima A, Bach L, Morin H, et al. (2010) Very-long-chain fatty acids are involved in polar auxin transport and developmental patterning in *Arabidopsis*. Plant Cell **22**(2): 364–375

Samuels L, Kunst L, Jetter R (2008) Sealing plant surfaces: cuticular wax formation by epidermal cells. Annu Rev Plant Biol **59**(1): 683–707

Sauer M, Kleine-Vehn J (2019) PIN-FORMED and PIN-LIKES auxin transport facilitators. Development **146**(15): dev168088

Sauveplane V, Kandel S, Kastner PE, Ehlting J, Compagnon V, Werck-Reichhart D, Pinot F (2009) *Arabidopsis thaliana* CYP77A4 is the first cytochrome P450 able to catalyze the epoxidation of free fatty acids in plants. FEBS J **276**(3): 719–735

Savaldi-Goldstein S, Chory J (2008) Growth coordination and the shoot epidermis. Curr Opin Plant Biol **11**(1): 42–48

Schmidt A (1924) Histologische studien an phanerogamen vegetationspunkten. Bot Arch **8**: 345–404

Schnurr J, Shockey J, Browse J (2004) The acyl-CoA synthetase encoded by *LACS2* is essential for normal cuticle development in *Arabidopsis*. Plant Cell **16**(3): 629–642

Schrick K, Mayer U, Martin G, Bellini C, Kuhnt C, Schmidt J, Jürgens G (2002) Interactions between sterol biosynthesis genes in embryonic development of *Arabidopsis*. Plant J **31**(1): 61–73

Serra O, Soler M, Hohn C, Franke R, Schreiber L, Prat S, Molinas M, Figueras M (2009) Silencing of *StKCS6* in potato periderm leads to reduced chain lengths of suberin and wax compounds and increased peridermal transpiration. J Exp Bot **60**(2): 697–707

Shani E, Burko Y, Ben-Yaakov L, Berger Y, Amsellem Z, Goldshmidt A, Sharon E, Ori N (2009) Stage-specific regulation of *Solanum lycopersicum* leaf maturation by class 1 KNOTTED1-LIKE HOMEOBOX proteins. Plant Cell **21**(10): 3078–3092

Shapiro BE, Tobin C, Mjolsness E, Meyerowitz EM (2015) Analysis of cell division patterns in the *Arabidopsis* shoot apical meristem. Proc Natl Acad Sci U S A **112**(15): 4815–4820

Shi J, Dong J, Xue J, Wang H, Yang Z, Jiao Y, Xu L, Huang H (2017) Model for the role of auxin polar transport in patterning of the leaf adaxial-abaxial axis. Plant J **92**(3): 469–480

Shockey JM, Fulda MS, Browse JA (2002) Arabidopsis contains nine long-chain acyl-coenzyme A synthetase genes that participate in fatty acid and glycerolipid metabolism. Plant Physiol **129**(4): 1710–1722

Shwartz I, Levy M, Ori N, Bar M (2016) Hormones in tomato leaf development. Dev Biol **419**(1): 132–142

Sussex IM (1989) Developmental programming of the shoot meristem. Cell **56**(2): 225–229

Tadege M, Wen JQ, He J, Tu HD, Kwak Y, Eschstruth A, Cayrel A, Endre G, Zhao PX, Chabaud M, et al. (2008) Large-scale insertional mutagenesis using the *Tnt1* retrotransposon in the model legume *Medicago truncatula*. Plant J **54**(2): 335–347

Takasugi T, Ito Y (2011) Altered expression of auxin-related genes in the fatty acid elongase mutant oni1 of rice. Plant Signal Behav **6**(6): 887–888

Tanaka H, Watanabe M, Sasabe M, Hiroe T, Tanaka T, Tsukaya H, Ikezaki M, Machida C, Machida Y (2007) Novel receptor-like kinase ALE2 controls shoot development by specifying epidermis in *Arabidopsis*. Development **134**(9): 1643–1652

Tanaka T, Tanaka H, Machida C, Watanabe M, Machida Y (2004) A new method for rapid visualization of defects in leaf cuticle reveals five intrinsic patterns of surface defects in *Arabidopsis*. Plant J **37**(1): 139–146

Tang D, Simonich MT, Innes RW (2007) Mutations in LACS2, a long-chain acyl-coenzyme A synthetase, enhance susceptibility to avirulent *Pseudomonas syringae* but confer resistance to *Botrytis cinerea* in *Arabidopsis*. Plant Physiol **144**(2): 1093–1103

Trenkamp S, Martin W, Tietjen K (2004) Specific and differential inhibition of very-long-chain fatty acid elongases from *Arabidopsis thaliana* by different herbicides. Proc Natl Acad Sci U S A **101**(32): 11903–11908

Verdoucq L, Grondin A, Maurel C (2008) Structure-function analysis of plant aquaporin AtPIP2;1 gating by divalent cations and protons. Biochem J **415**(3): 409–416

Vittorioso P, Cowling R, Faure JD, Caboche M, Bellini C (1998) Mutation in the Arabidopsis *PASTICCINO1* gene, which encodes a new FK506-binding protein-like protein, has a dramatic effect on plant development. Mol Cell Biol **18**(5): 3034–3043

Wang CJ, Wen JQ, Tadege M, Li GM, Liu Y, Mysore KS, Ratet P, Chen RJ (2008) Control of compound leaf development by *FLORICAULA/LEAFY* ortholog *SINGLE LEAFLET1* in *Medicago truncatula*. Plant Physiol **146**(4): 1759–1772

Watanabe M, Tanaka H, Watanabe D, Machida C, Machida Y (2004) The ACR4 receptor-like kinase is required for surface formation of epidermis-related tissues in *Arabidopsis thaliana*. Plant J **39**(3): 298–308

Wellesen K, Durst F, Pinot F, Benveniste I, Nettesheim K, Wisman E, Steiner-Lange S, Saedler H, Yephremov A (2001) Functional analysis of the *LACERATA* gene of *Arabidopsis* provides evidence for different robes of fatty acid omega-hydroxylation in development. Proc Natl Acad Sci U S A **98**(17): 9694–9699

Weng H, Molina I, Shockey J, Browse J (2010) Organ fusion and defective cuticle function in a *lacs1 lacs2* double mutant of *Arabidopsis*. Planta **231**(5): 1089–1100

Willemsen V (2003) Cell polarity and PIN protein positioning in Arabidopsis require *STEROL METHYLTRANSFERASE1* function. Plant Cell **15**(3): 612–625

Wu L, Zhou ZY, Zhang CG, Chai J, Zhou Q, Wang L, Hirnerová E, Mrvková M, Novák O, Guo GQ (2015) Functional roles of three cutin biosynthetic acyltransferases in cytokinin responses and skotomorphogenesis. PLoS ONE **10**(3): e0121943

Wu R, Li S, He S, Wassmann F, Yu C, Qin G, Schreiber L, Qu LJ, Gu H (2011) CFL1, A WW domain protein, regulates cuticle development by modulating the function of HDG1, a class IV homeodomain transcription factor, in rice and *Arabidopsis*. Plant Cell **23**(9): 3392–3411

Wudick MM, Li X, Valentini V, Geldner N, Chory J, Lin J, Maurel C, Luu DT (2015) Subcellular redistribution of root aquaporins induced by hydrogen peroxide. Mol Plant **8**(7): 1103–1114

Xiao FM, Goodwin SM, Xiao YM, Sun ZY, Baker D, Tang XY, Jenks MA, Zhou JM (2004) *Arabidopsis CYP86A2* represses *Pseudomonas syringae* type III genes and is required for cuticle development. EMBO J **23**(14): 2903–2913

Xiong Y, Jiao Y (2019) The diverse roles of auxin in regulating leaf development. Plants (Basel) **8**(7): 243

Yadav RK, Tavakkoli M, Xie M, Girke T, Reddy GV (2014) A high-resolution gene expression map of the *Arabidopsis shoot* meristem stem cell niche. Development **141**(13): 2735–2744

Yeats TH, Rose JKC (2013) The formation and function of plant cuticles. Plant Physiol **163**(1): 5–20

Yephremov A, Wisman E, Huijser P, Huijser C, Wellesen K, Saedler H (1999) Characterization of the *FIDDLEHEAD* gene of *Arabidopsis* reveals a link between adhesion response and cell differentiation in the epidermis. Plant Cell **11**(11): 2187–2201

Yoo YJ, Lee HK, Han W, Kim DH, Lee MH, Jeon J, Lee DW, Lee J, Lee Y, Lee J, et al. (2016) Interactions between transmembrane helices within monomers of the aquaporin AtPIP2;1 play a crucial role in tetramer formation. Mol Plant **9**(7): 1004–1017

Zheng H, Rowland O, Kunst L (2005) Disruptions of the Arabidopsis Enoyl-CoA reductase gene reveal an essential role for very-long-chain fatty acid synthesis in cell expansion during plant morphogenesis. Plant Cell **17**(5): 1467–1481

Zhou CN, Han L, Fu CX, Wen JQ, Cheng XF, Nakashima J, Ma JY, Tang YH, Tan Y, Tadege M, et al. (2013) The *trans*-acting short interfering RNA3 pathway and NO APICAL MERISTEM antagonistically regulate leaf margin development and lateral organ separation, as revealed by analysis of an *argonaute7/lobed leaflet1* mutant in *Medicago truncatula*. Plant Cell **25**(12): 4845–4862

Zhou CN, Han L, Hou CY, Metelli A, Qi LY, Tadege M, Mysore KS, Wang ZY (2011) Developmental analysis of a *Medicago truncatula smooth leaf margin1* mutant reveals context-dependent effects on compound leaf development. Plant Cell **23**(6): 2106–2124

Zhou CN, Han L, Li GF, Chai MF, Fu CX, Cheng XF, Wen JQ, Tang YH, Wang ZY (2014) STM/BP-like KNOXI is uncoupled from ARP in the regulation of compound leaf development in *Medicago truncatula*. Plant Cell **26**(4): 1464–1479